Active vibration control of thin constrained composite damping plates with double piezoelectric layers

Xiongtao Cao [1,2] [*], **Gregor Tanner** [1], **Dimitrios Chronopoulos** [3]

1. School of Mathematical Sciences, University of Nottingham, University Park, NG7 2RD, UK

2. Laboratory of Marine Power Cabins, Shanghai Maritime University, Shanghai, China

3. Institute for Aerospace Technology and The Composites Group, University of Nottingham, University Park, NG7 2RD, UK

August 30, 2019

[*]Corresponding author, caolin1324@126.com

Cover Letter

Dear Editor,

Free and forced vibrations of thin constrained damping composite plates with double piezoelectric layers are investigated in the wavenumber domain. The electric potential equations are solved for two piezoelectric layers with three passive control methods and one active control method, and implicit governing equations described by a loading vector and a five dimensional spectral matrix for the smart composite plates are obtained. The formulae in this work are verified by comparing the present results with those in the literature. Three passive control methods, i.e., two smart layers with the closed circuit conditions, open circuit conditions and an dielectric slab, do not distinctly change the natural frequencies and loss factors of the composite plate since only a small portion of mechanical energy is converted into electrical energy. Proportional derivative active control notably affects the natural frequencies and loss factors of the composite plate. Forced vibrations of the composite plates are characterized by plane power spectral density (PPSD), radial power spectral density (RPSD), cylindrical-wave spectral density (CSD) and phase angles of elastic waves for transverse displacements. We introduce three quantities (RPSD, CSD and phase angles of the propagating waves) in this paper, which is different from our former studies on sound and vibration of stiffened composite plates. Interesting phenomena and mechanisms are explained in detail. The derivative gain of active control has important effects on vibration suppression performance of the smart composite plates.

Yours sincerely

Xiongtao Cao

Highlights

1. Free and forced vibrations of the smart sandwich plates are analytically investigated in the wavenumber domain.

2. Three-dimensional electric potential equations of the two piezoelectric layers with four kinds of circuit boundary conditions are solved.

3. Cylindrical-wave spectral density is used to analyze far-field vibration of the smart composite plates.

Abstract

Vibrations and the damping behaviour of thin constrained composite plates with double piezoelectric layers are analytically explored by using Fourier transformation and classical laminated plate theory. Electric potential equations in the double piezoelectric layers are solved with respect to closed and open circuit boundary conditions, an exterior dielectric slab and active control. The natural frequencies and loss factors of the constrained smart composite plates with passive control methods are not notably changed in comparison with those of the constrained composite plates without piezoelectric effects since vibrational energy does not efficiently convert to electrical energy. The loss factors of the composite plates with active constrained damping increase and the natural frequencies have significant variations as the proportional derivative gains increase. Transverse displacement power spectra of the piezoelectric composite plates with active control are compared with those of the piezoelectric composite plates with passive control showing that active control has the best suppression performance of vibrations for the constrained laminated plates with double piezoelectric layers. Radial power spectral density, phase angles and cylindrical-wave power spectral density are calculated. Interesting patterns of wave propagation are explained when plane wave expansion is used to obtain Bessel cylindrical waves.

Keywords: constrained damping layer; piezoelectric layer; composite plate; vibration; cylindrical wave

1 Introduction

Passive constrained damping layers have excellent performance with respect to vibration suppression of composite plates and shells in marine and aeronautic engineering. Piezoelectric constrained damping layers can further reduce vibration of the composite structures. Smart constrained damping composites with superior sense and drive properties have attracted a lot of research interests recently [1]. One kind of viscoelastic layer is constrained damping, where the layer is sandwiched by two face panels. It is in contrast to free damping, where the layer directly covers the surface of the host structure. Free damping layers typically induce a smaller global damping loss factor for the assembled structure. Damping materials for the constrained damping layer are often made of butyl rubber while typical materials for free damping layers are polymerized by chlorosulfonated polyethylene rubber.

Great efforts were devoted to studying the vibrations of constrained piezoelectric composite damping plates. Shen [2] analytically derived the governing equations and boundary conditions of constrained damping sandwich shells using the three-dimensional piezoelectric elastic theory but numerical results for composite shells with a piezoelectric constrained damping layer were not presented. Zhang and Zhang [3] studied active and passive vibration control of a host plate with local piezoelectric constrained damping layer via the Galerkin method. The electric potential in the piezoelectric layer was described by the external control voltage. Gao and Shen [4] derived the governing equations of constrained composite plates with a single piezoelectric layer according to the D'Alembert principle and classical laminated plate theory. Three-dimensional electric potential equations of the piezoelectric laminas were solved with closed and open circuit boundary conditions. Natural frequencies and loss factors of the sandwich plates with a single piezoelectric layer were given. Similarly, Park and Baz [5] presented the equations of motion for the composite plates with a single active constrained damping layer on the basis of the classical laminated plate theory and investigated transient vibration of the composite plates. However, electric potential of the piezoelectric layer was modelled by the same method as shown in [3] and proportional derivative active control was used. Yuan et al. [6] developed the first-order differential equations to semi-analytically solve the vibrational responses of the circular cylindrical shells with active constrained damping layer based on the transfer matrix method [7]. The electrodes of a piezoelectric layer were divided into several segments in the circumferential direction and the electric potential in the piezoelectric layer was assumed to be the external input electric

potential. The topological configurations of the electrodes affected the vibration control of the composite plates and shells with piezoelectric lamina. Piezoelectric fibre laminas were driven by the interdigitated electrodes in order to excite elastic waves [8–10]. Akop'yan et al. [11] explored the vibrations of piezoelectric elements with nonuniform electrode connections. The host plates were treated with periodic arrays of shunted piezoelectric patches in order to control sound radiation and transmission of the composite plates [12–16]. Numerical and analytical models were established by the wave finite element method [12] and the smeared piezoelectric patch approach [13, 14, 16]. The finite element method was employed to examine active vibration control of the composite plates and shells with piezoelectric constrained damping layers [17–22]. Proportional derivative feedback control [18, 20–22] and linear quadratic regulator (LQR) optimal control [19] were applied to the piezoelectric layers. Carra and Amabili [23] investigated experimentally a rectangular aluminium plate vibrating in air or in contact with water and used the filtered-x least mean square (FXLMS) adaptive feedforward algorithm to realize structural vibration control of the vibration modes. Ferrari and Amabili [24] experimentally examined active vibration control of a free rectangular sandwich plate using the positive position feedback (PPF) algorithm. The amplitude reduction achieved by the non-collocated configuration was much larger than that obtained by the nearby collocated one. Yang et al. [25] investigated vibrations and damping performance of the hybrid carbon fibre composite pyramidal truss sandwich plates with viscoelastic layers embedded in the face sheets using the modal strain energy approach.

Many studies on vibration control of composite plates and shells with two piezoelectric layers were performed using analytical and numerical methods [26–43]. Ray [27] derived the governing equations of laminated shells with piezoelectric sensors and actuator layers according to the classical laminated shell theory and assumed that the electric potential in the actuator layer was a linear distribution through the thickness direction. LQR control was applied and the electric potential equation of the sensor layer was neglected. Song et al. [33] presented an active aeroelastic flutter analysis and vibration control of supersonic composite laminated plate using classical laminated plate theory, and the electric potential was described by the same method as in Refs. [3, 6]. Using the same theory, Arshid et al. [43] studied free vibrations of saturated porous functionally graded circular plates integrated with piezoelectric actuators via the differential quadrature method. The governing equations of the composite thick circular plates [26], annular functionally graded plates [28] and functionally graded laminated cylindrical shells [29]

with double piezoelectric layers were derived by using the first-order shear deformable plate theory and layerwise quadratic distribution approximations of the electric potentials. Based on the higher-order shear deformation theory, linear and nonlinear vibrations of the composite plates and shells with two piezoelectric layers were analyzed [30, 31, 35, 38, 40, 42] and electric potential variations in the smart active layers were expressed by the assumed distribution functions along the thickness direction.

Vibrations and sound radiation of smart cylindrical shells with two piezoelectric layers were explored [32, 34, 36, 39] in the state space. The composite cylindrical shells were required to be divided into several thin cylinders for the state space method. The effects of the temperature field on the vibrations of piezoelectric composite plates and shells were taken into account [29, 39–41]. Piezoelectric constants and permittivity coefficients of the piezoelectric laminas were significantly influenced by the temperature field which was produced by the external driving voltage as a result of electric energy dissipation. Piezoelectric effects disappeared when the temperature was above the Curie temperature point of the piezoelectric materials. The experiments of active vibration control for the composite plates and shells with arrays of piezoelectric patches were performed and the features of active control were demonstrated [19, 44, 45]. First-order and third-order shear deformation theories were employed to establish the governing equations of the constrained sandwich damping plates and shells [46–50]. These shear deformable models [46, 49, 50] could be utilized in a broad frequency range and normal deformation of the viscoelastic core in the thickness direction needed to be taken into account in the medium and high frequency range. Vibrations of the composite plates with a periodic perforated viscoelastic damping layer were explored by asymptotic analysis and the finite element method [51–53]. Vibrations of the constrained damping composite circular and annular plates were examined on the basis of the assumed-mode method and the finite element method [54–56]. The dynamic stability of the rotating sandwich annular plates with viscoelastic core was analyzed by the finite element method and the Galerkin method [57, 58].

Analytical solutions to the vibrations of constrained rectangular and circular composite plates with double piezoelectric layers are rare. Only some analytical, semi-analytical and numerical work examined the vibrations of constrained composite damping plates with a single piezoelectric layer [2–5]. Cao et al. [59] investigated active control of sound radiation from laminated cylindrical shells with a single piezoelectric layer and periodic segmented electrodes in the wavenumber domain. Research on the vibrational and acoustic features of the piezo-

electric composite plates and shells is very limited in the wavenumber domain. The implicit governing equations of the constrained composite damping plates with arbitrary smart layers are derived by using the two-dimensional Fourier transform in the present work. Free and forced vibrations of the constrained composite plates with two piezoelectric layers are analyzed via three passive control methods and one active control method. The natural frequencies and loss factors of the smart composite plates are given. Plane wave expansion is performed through a cylindrical wave transform. The far-field cylindrical-wave power spectral density, radial power spectral density and phase angle pattern of the transverse displacement for the constrained composite plates with double piezoelectric layers are explored.

2 Theoretical formulation of the wavenumber model

An infinite thin constrained composite damping plate with double piezoelectric layers is illustrated in Fig. 1. The viscoelastic core is sandwiched between two piezoelectric laminated face plates. The upper piezoelectric laminated panel is the constraining plate and the lower piezoelectric laminated panel is the host plate in Fig. 1. The polarization direction of the two piezoelectric layers is along the z axis. A sensor layer is attached at the host plate and an actuator layer is included in the constraining plate. Electric boundary conditions of the double piezoelectric layers can be open or closed circuit. Two piezoelectric layers can also be connected by an external dielectric slab with uniform resistances and inductances. The dielectric slab with periodic electrodes and the equivalent circuit architecture of one cell are shown in Fig. 2. Similar electrode segments are uniformly distributed on the outer surfaces of the two piezoelectric layers and the electrodes of the piezoelectric layers are connected with those of the slab according to the same in-plane location. The voltage of the sensor layer at the lower surface of the host plate is fed back into the actuator layer by the external power amplifiers when an active control method is used. The factor $\mathrm{e}^{-\mathrm{i}\omega t}$ is suppressed throughout the paper.

The mechanical models of the composite plates and shells can be established by several plate and shell theories. Vibrations of the active constrained sandwich plate were studied on the basis of the classical as well as the layer-wise laminated plate theory by Park and Baz [60], which was validated by the experiments in the low frequency range. Cao and Hua [61] showed that the classical and the first-order shear deformable plate theories yielded the same equations of motion for the isotropic moderately thick plate in the low frequency range. Chronopoulos and

Ichchou et al. [62] used the wave finite element approach to calculate the dispersion curves of a thin orthotropic plate and compared the results with those given by the classical plate theory. It was shown that the orthotropic plate modelled by the classical plate theory was valid from the low to the high frequency range. The classical plate theory with von Kármán strains, the first-order shear deformation theory and the third-order shear deformation theory were compared with respect to nonlinear vibrations of the laminated composite rectangular plates by Amabili and Farhadi [63]. Difference of nonlinear vibration arose for the thick laminated composite plates with a ratio of thickness to length equal to 0.1. There was negligible difference for the thin laminated composite plates with a ratio of thickness to length equal to 0.01. Amabili [64] studied nonlinear vibrations for the laminated circular cylindrical shells using the Novozhilov classical, higher-order shear deformation and Amabili-Reddy [65] shell theories. The Amabili-Reddy and Novozhilov theories gave good results for the thin laminated shells with a ratio of thickness to radius equal to 0.02. For the thick laminated shells with a ratio equal to 0.2, the Amabili-Reddy theory should be used in order to obtain accurate results. Free and forced vibrations of thick laminated composite plates with a ratio of thickness to length equal to 0.1 predicted by the classical and shear deformation plate theories had some discrepancies [66–68]. Liu [69] pointed out that classical plate theory could be applied to smart composite plates with a ratio of thickness to length less than 0.1. Classical plate theory which is simpler than shear deformation plate theory can be used to study the vibrations of thin composite plates and shells in the low and medium frequency range. Active control of the piezoelectric layers for constrained sandwich plates is utilized in the low frequency range since the performance of vibration suppression for the passive viscoelastic damping layer is poor in this frequency band. In the medium and high frequency range, vibration attenuation performance of the viscoelastic damping layer is excellent and active control is not necessary. Classical plate theory is used to establish the vibration model of thin constrained composite damping plates with double piezoelectric layers in this work.

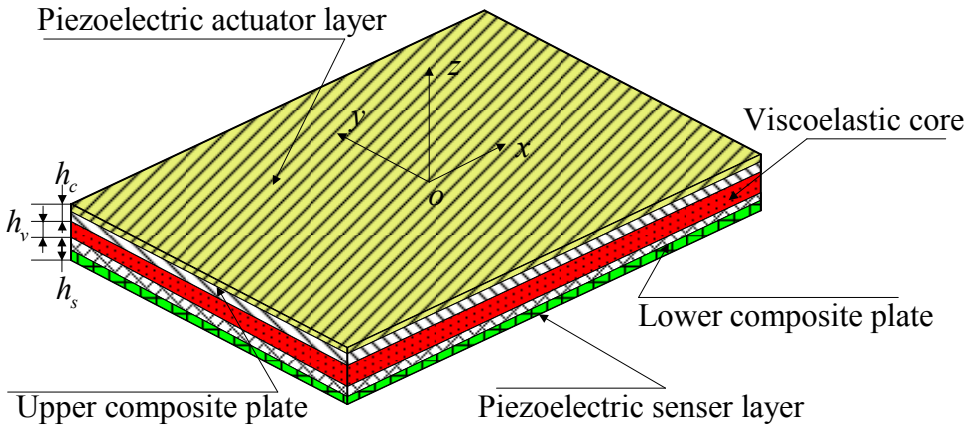

Figure 1: Thin constrained composite plate with double piezoelectric layers

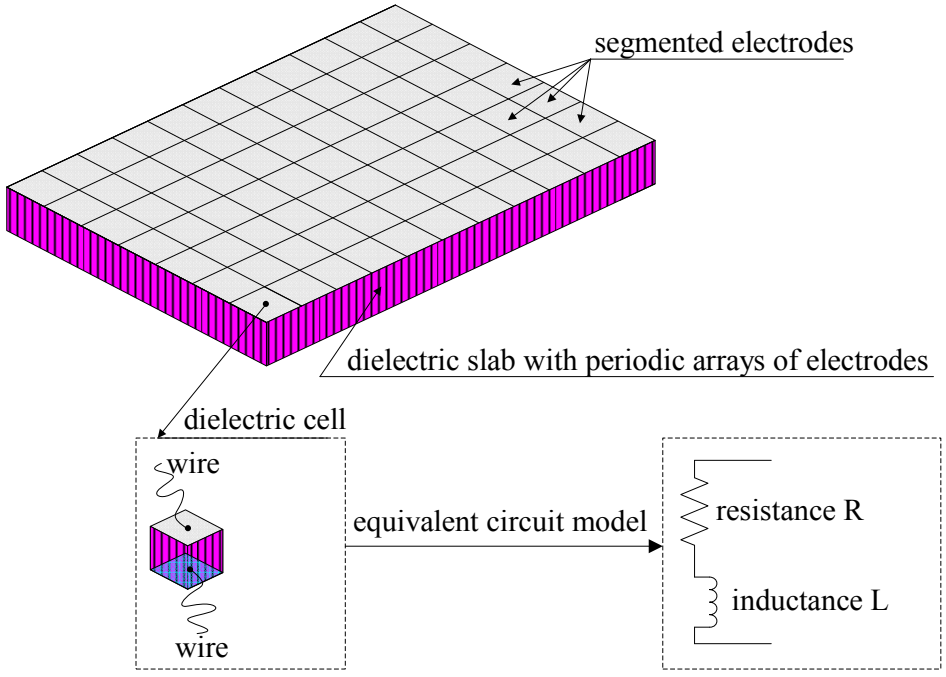

Figure 2: Dielectric slab with periodic arrays of the electrodes and the equivalent circuit model of a cell

2.1 Governing equations of the constrained composite plates with double piezoelectric layers

2.1.1 Motion of smart sandwich plates

2.1.1.1 Displacement fields of the composite plates The transverse displacements of two-face plates are assumed to be the same. In-plane and normal deformation of the viscoelastic core is neglected and only the transverse shear deformation of the viscoelastic layer is taken into account. These theoretical conditions are similar to those in Refs. [60, 70]. The displacements of the constrained composite plates are described by

$$\begin{aligned}
U_j^{(s)}(x,y,z) &= u_j^{(s)}(x,y) + \left(z + \frac{h_v + h_s}{2}\right)\beta_j^{(s)}(x,y), \\
U_j^{(v)}(x,y,z) &= u_j^{(v)}(x,y) + z\beta_j^{(v)}(x,y), \\
U_j^{(c)}(x,y,z) &= u_j^{(c)}(x,y) + \left(z - \frac{h_v + h_c}{2}\right)\beta_j^{(c)}(x,y), \\
U_3(x,y) &= u_3(x,y),
\end{aligned} \tag{1}$$

where the subscript j is 1 or 2 denoting the translational and angular displacements in the x and y directions, respectively. z is the global transverse coordinate of the composite plate. The superscripts s, v and c denote physical quantities associated with the host plate, viscoelastic layer and constraining plate. $U_j^{(s)}$, $U_j^{(v)}$ and $U_j^{(c)}$ are the in-plane displacements of the composite plates. u_3 is the transverse displacement of the sandwich plate. $u_j^{(s)}(x,y)$ and $u_j^{(c)}(x,y)$ are the displacements of the medium surfaces for the two face plates. $\beta_j^{(c)}(x,y)$ and $\beta_j^{(s)}(x,y)$ are the rotational angles of the upper and lower laminated plates. $u_j^{(v)}(x,y)$ and $\beta_j^{(v)}(x,y)$ are the displacements and rotational angles of the medium surface for the damping core. According to classical laminated plate theory, one obtains

$$\beta_1^{(c)} = -\frac{\partial u_3}{\partial x},\ \beta_1^{(s)} = -\frac{\partial u_3}{\partial x},\ \beta_2^{(c)} = -\frac{\partial u_3}{\partial y},\ \beta_2^{(s)} = -\frac{\partial u_3}{\partial y}. \tag{2}$$

Layerwise displacements of the piezoelectric composite plate with constrained damping layer are shown in Fig. 3, which is similar to the displacement compatibility relation for a sandwich cylindrical shell with constrained damping core given by Chen and Huang [71]. Z is the local transverse coordinate of the viscoelastic layer and two face panels in Fig. 3. Displacement boundary conditions among the constraining plate, viscoelastic core and host plate can be

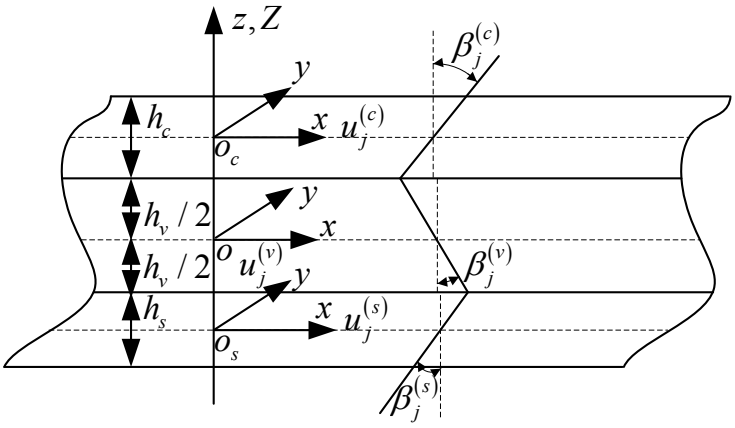

Figure 3: Layerwise displacements and local coordinate system of constrained composite damping plate with double piezoelectric layers

described by

$$u_1^{(v)} = \frac{1}{2}\left(u_1^{(c)} - \frac{h_c}{2}\beta_1^{(c)} + u_1^{(s)} + \frac{h_s}{2}\beta_1^{(s)}\right),\ u_2^{(v)} = \frac{1}{2}\left(u_2^{(c)} - \frac{h_c}{2}\beta_2^{(c)} + u_2^{(s)} + \frac{h_s}{2}\beta_2^{(s)}\right), \tag{3}$$

$$\beta_1^{(v)} = \frac{1}{h_v}\left(u_1^{(c)} - \frac{h_c}{2}\beta_1^{(c)} - u_1^{(s)} - \frac{h_s}{2}\beta_1^{(s)}\right),\ \beta_2^{(v)} = \frac{1}{h_v}\left(u_2^{(c)} - \frac{h_c}{2}\beta_2^{(c)} - u_2^{(s)} - \frac{h_s}{2}\beta_2^{(s)}\right). \tag{4}$$

Substituting Eq. (2) into Eqs. (3) and (4), one obtains

$$u_1^{(v)} = \frac{1}{2}\left(u_1^{(c)} + u_1^{(s)} + \frac{h_c - h_s}{2}\frac{\partial u_3}{\partial x}\right), u_2^{(v)} = \frac{1}{2}\left(u_2^{(c)} + u_2^{(s)} + \frac{h_c - h_s}{2}\frac{\partial u_3}{\partial y}\right), \tag{5}$$

$$\beta_1^{(v)} = \frac{1}{h_v}\left(u_1^{(c)} + \frac{h_c + h_s}{2}\frac{\partial u_3}{\partial x} - u_1^{(s)}\right), \beta_2^{(v)} = \frac{1}{h_v}\left(u_2^{(c)} + \frac{h_c + h_s}{2}\frac{\partial u_3}{\partial y} - u_2^{(s)}\right). \tag{6}$$

Transverse shear strains of the viscoelastic core are expressed by

$$\varepsilon_{xz}^{(v)} = \frac{\partial u_3}{\partial x} + \beta_1^{(v)}, \varepsilon_{yz}^{(v)} = \frac{\partial u_3}{\partial y} + \beta_2^{(v)}. \tag{7}$$

Transverse shear stresses of the viscoelastic core are given by

$$\sigma_{xz}^{(v)} = G_v\left(\frac{\partial u_3}{\partial x} + \beta_1^{(v)}\right), \sigma_{yz}^{(v)} = G_v\left(\frac{\partial u_3}{\partial y} + \beta_2^{(v)}\right), \tag{8}$$

where G_v is the complex shear modulus. Displacement-strain relation of the constraining laminated plate with respect to the $l-$th orthotropic layer is addressed by

$$\begin{bmatrix} \varepsilon_{xx}^{(l,c)} \\ \varepsilon_{yy}^{(l,c)} \\ \varepsilon_{xy}^{(l,c)} \end{bmatrix} = \begin{bmatrix} \varepsilon_{xx}^{(l,0)} \\ \varepsilon_{yy}^{(l,0)} \\ \varepsilon_{xy}^{(l,0)} \end{bmatrix} + Z \begin{bmatrix} \varepsilon_{xx}^{(l,1)} \\ \varepsilon_{yy}^{(l,1)} \\ \varepsilon_{xy}^{(l,1)} \end{bmatrix}. \tag{9}$$

For the constraining plate and the host plate, Z is defined by $z-(h_v+h_c)/2$ and $z+(h_v+h_s)/2$, respectively. $\varepsilon_{xx}^{(l,c)}$, $\varepsilon_{yy}^{(l,c)}$ and $\varepsilon_{xy}^{(l,c)}$ are the normal strains in the x and y directions, and in-plane shear strain of the $l-$th lamina, respectively. $\varepsilon_{xx}^{(l,0)}$, $\varepsilon_{yy}^{(l,0)}$, $\varepsilon_{xy}^{(l,0)}$, $\varepsilon_{xx}^{(l,1)}$, $\varepsilon_{yy}^{(l,1)}$ and $\varepsilon_{xy}^{(l,1)}$ are the reduced strains of the $l-$th lamina and given by

$$\begin{aligned} \varepsilon_{xx}^{(l,0)} &= \frac{\partial u_1^{(c)}}{\partial x}, \varepsilon_{yy}^{(l,0)} = \frac{\partial u_2^{(c)}}{\partial y}, \varepsilon_{xy}^{(l,0)} = \frac{\partial u_1^{(c)}}{\partial y} + \frac{\partial u_2^{(c)}}{\partial x}, \\ \varepsilon_{xx}^{(l,1)} &= -\frac{\partial^2 u_3}{\partial x^2}, \varepsilon_{yy}^{(l,1)} = -\frac{\partial^2 u_3}{\partial y^2}, \varepsilon_{xy}^{(l,1)} = -2\frac{\partial^2 u_3}{\partial x \partial y}. \end{aligned} \tag{10}$$

One can obtain the displacement-strain relation of the host plate with respect to the $l-$th orthotropic layer if the superscript c is replaced with s in Eqs. (9) and (10).

2.1.1.2 Constitutive equations Constitutive relations of the $l-$th orthotropic layer for the constraining plate with piezoelectric effects are described by

$$\begin{bmatrix} \sigma_{xx}^{(l,c)} \\ \sigma_{yy}^{(l,c)} \\ \tau_{xy}^{(l,c)} \end{bmatrix} = \begin{bmatrix} \bar{Q}_{11}^{(l,c)} & \bar{Q}_{12}^{(l,c)} & \bar{Q}_{16}^{(l,c)} \\ \bar{Q}_{12}^{(l,c)} & \bar{Q}_{22}^{(l,c)} & \bar{Q}_{26}^{(l,c)} \\ \bar{Q}_{16}^{(l,c)} & \bar{Q}_{26}^{(l,c)} & \bar{Q}_{66}^{(l,c)} \end{bmatrix} \begin{bmatrix} \varepsilon_{xx}^{(l,c)} \\ \varepsilon_{yy}^{(l,c)} \\ \varepsilon_{xy}^{(l,c)} \end{bmatrix} - \begin{bmatrix} 0 & 0 & \bar{e}_{31}^{(l,c)} \\ 0 & 0 & \bar{e}_{32}^{(l,c)} \\ 0 & 0 & \bar{e}_{36}^{(l,c)} \end{bmatrix} \begin{bmatrix} E_1^{(l,c)} \\ E_2^{(l,c)} \\ E_3^{(l,c)} \end{bmatrix}, \tag{11}$$

$$\begin{bmatrix} D_1^{(l,c)} \\ D_2^{(l,c)} \\ D_3^{(l,c)} \end{bmatrix} = \begin{bmatrix} 0 & 0 & 0 \\ 0 & 0 & 0 \\ \bar{e}_{31}^{(l,c)} & \bar{e}_{32}^{(l,c)} & \bar{e}_{36}^{(l,c)} \end{bmatrix} \begin{bmatrix} \varepsilon_{xx}^{(l,c)} \\ \varepsilon_{yy}^{(l,c)} \\ \varepsilon_{xy}^{(l,c)} \end{bmatrix} + \begin{bmatrix} \bar{\xi}_{11}^{(l,c)} & \bar{\xi}_{12}^{(l,c)} & 0 \\ \bar{\xi}_{12}^{(l,c)} & \bar{\xi}_{22}^{(l,c)} & 0 \\ 0 & 0 & \bar{\xi}_{33}^{(l,c)} \end{bmatrix} \begin{bmatrix} E_1^{(l,c)} \\ E_2^{(l,c)} \\ E_3^{(l,c)} \end{bmatrix}, \tag{12}$$

where $\bar{Q}_{ij}^{(l,c)}$, $\bar{e}_{ij}^{(l,c)}$ and $\bar{\xi}_{ij}^{(l,c)}$ are the reduced stiffnesses, piezoelectric coefficients and permittivity coefficients, respectively. $E_1^{(l,c)}$, $E_2^{(l,c)}$ and $E_3^{(l,c)}$ are the electric field intensities, given by

$$\begin{bmatrix} E_1^{(l,c)} & E_2^{(l,c)} & E_3^{(l,c)} \end{bmatrix}^{\mathrm{T}} = -\begin{bmatrix} \frac{\partial \Phi^{(l,c)}}{\partial x} & \frac{\partial \Phi^{(l,c)}}{\partial y} & \frac{\partial \Phi^{(l,c)}}{\partial z} \end{bmatrix}^{\mathrm{T}}, \tag{13}$$

where $\Phi^{(l,c)}$ is the electric potential of the $l-$th orthotropic layer. Eqs. (11) and (12) can be

expressed in terms of the matrices

$$\begin{aligned}\boldsymbol{\sigma}_l^{(c)} &= \mathbf{Q}_l^{(c)}\boldsymbol{\varepsilon}_l^{(c)} - \mathbf{e}_l^{(c)}\mathbf{E}_l^{(c)},\\ \mathbf{D}_l^{(c)} &= \left(\mathbf{e}_l^{(c)}\right)^{\mathrm{T}}\boldsymbol{\varepsilon}_l^{(c)} + \boldsymbol{\xi}_l^{(c)}\mathbf{E}_l^{(c)},\end{aligned} \tag{14}$$

where the stress vector $\boldsymbol{\sigma}_l^{(c)}$, strain vector $\boldsymbol{\varepsilon}_l^{(c)}$, electric displacement vector $\mathbf{D}_l^{(c)}$ and electric field intensity vector $\mathbf{E}_l^{(c)}$ are denoted by

$$\begin{aligned}\boldsymbol{\sigma}_l^{(c)} &= \begin{bmatrix} \sigma_{xx}^{(l,c)} & \sigma_{yy}^{(l,c)} & \tau_{xy}^{(l,c)} \end{bmatrix}^{\mathrm{T}}, \boldsymbol{\varepsilon}_l^{(c)} = \begin{bmatrix} \varepsilon_{xx}^{(l,c)} & \varepsilon_{yy}^{(l,c)} & \varepsilon_{xy}^{(l,c)} \end{bmatrix}^{\mathrm{T}},\\ \mathbf{D}_l^{(c)} &= \begin{bmatrix} D_1^{(l,c)} & D_2^{(l,c)} & D_3^{(l,c)} \end{bmatrix}^{\mathrm{T}}, \mathbf{E}_l^{(c)} = \begin{bmatrix} E_1^{(l,c)} & E_2^{(l,c)} & E_3^{(l,c)} \end{bmatrix}^{\mathrm{T}}.\end{aligned} \tag{15}$$

Similarly, constitutive relation of the l−th orthotropic layer for the host plate with piezoelectric effects can be described by (14), and the superscript c is replaced with s.

2.1.1.3 Hamilton's principle Neglecting the rotational inertia, one obtains the kinetic energy of the constraining plate

$$K_c = \frac{1}{2}\sum_{l=1}^{N_c}\int_{\Omega_l^{(c)}} \rho_l^{(c)}\left(\left(\dot{u}_1^{(c)}\right)^2 + \left(\dot{u}_2^{(c)}\right)^2 + \dot{u}_3^2\right)\mathrm{d}v, \tag{16}$$

where $\rho_l^{(c)}$ is the density of the l−th orthotropic layer and the superscript dot denotes the derivative with respect to time. $\Omega_l^{(c)}$ is the volume domain of the l−th orthotropic layer and N_c denotes the layer counts of the constraining plate, respectively. Similarly, the kinetic energy of the host plate is expressed as

$$K_s = \frac{1}{2}\sum_{l=1}^{N_s}\int_{\Omega_l^{(s)}} \rho_l^{(s)}\left(\left(\dot{u}_1^{(s)}\right)^2 + \left(\dot{u}_2^{(s)}\right)^2 + \dot{u}_3^2\right)\mathrm{d}v, \tag{17}$$

where $\rho_l^{(s)}$ and $\Omega_l^{(s)}$ are the density and volume domain of the l−th orthotropic layer for the host plate. N_s denotes the layer counts of the host plate. The kinetic energy of the viscoelastic core is given by

$$K_v = \frac{1}{2}\int_{\Omega_v} \rho_v\left(\left(\dot{u}_1^{(v)}\right)^2 + \left(\dot{u}_2^{(v)}\right)^2 + \dot{u}_3^2\right)\mathrm{d}v, \tag{18}$$

where ρ_v and Ω_v are the density and volume domain of the viscoelastic core, respectively.

According to the extended Hamilton's principle, one obtains

$$\int_0^{t_1}\Bigg[\sum_{l=1}^{N_c}\int_{\Omega_l^{(c)}}\delta\left(\boldsymbol{\varepsilon}_l^{(c)}\right)^{\mathrm{T}}\left(\mathbf{Q}_l^{(c)}\boldsymbol{\varepsilon}_l^{(c)}-\mathbf{e}_l^{(c)}\mathbf{E}_l^{(c)}\right)-\delta\left(\mathbf{E}_l^{(c)}\right)^{\mathrm{T}}\left(\left(\mathbf{e}_l^{(c)}\right)^{\mathrm{T}}\boldsymbol{\varepsilon}_l^{(c)}+\xi_l\mathbf{E}_l^{(c)}\right)\mathrm{d}v$$
$$+\sum_{l=1}^{N_s}\int_{\Omega_l^{(s)}}\delta\left(\boldsymbol{\varepsilon}_l^{(s)}\right)^{\mathrm{T}}\left(\mathbf{Q}_l^{(s)}\boldsymbol{\varepsilon}_l^{(s)}-\mathbf{e}_l^{(s)}\mathbf{E}_l^{(s)}\right)-\delta\left(\mathbf{E}_l^{(s)}\right)^{\mathrm{T}}\left(\left(\mathbf{e}_l^{(s)}\right)^{\mathrm{T}}\boldsymbol{\varepsilon}_l^{(s)}+\xi_l\mathbf{E}_l^{(s)}\right)\mathrm{d}v$$
$$+\int_{\Omega_v}\left(\delta\varepsilon_{xz}^{(v)}\sigma_{xz}^{(v)}+\delta\varepsilon_{yz}^{(v)}\sigma_{yz}^{(v)}\right)\mathrm{d}v-\int\int\delta\mathbf{u}^{\mathrm{T}}\mathbf{F}\mathrm{d}x\mathrm{d}y-\delta K_c-\delta K_s-\delta K_v\Bigg]\mathrm{d}t=0, \quad (19)$$

where $\mathbf{u}$ and $\mathbf{F}$ are the displacement vector and external loading vector. Simplifying the first term on the left-hand side in Eq. (19), one obtains

$$\int_z\delta\left(\boldsymbol{\varepsilon}_l^{(c)}\right)^{\mathrm{T}}\left(\mathbf{Q}_l^{(c)}\boldsymbol{\varepsilon}_l^{(c)}-\mathbf{e}_l^{(c)}\mathbf{E}_l^{(c)}\right)\mathrm{d}z=\int_z\left(\mathbf{Q}_l^{(c)}\boldsymbol{\varepsilon}_l^{(c)}-\mathbf{e}_l^{(c)}\mathbf{E}_l^{(c)}\right)^{\mathrm{T}}\delta\left(\boldsymbol{\varepsilon}_l^{(c)}\right)\mathrm{d}z$$
$$=\left(\begin{bmatrix}u_1^{(c)}\\u_2^{(c)}\\u_3\end{bmatrix}^{\mathrm{T}}\mathbf{N}_c^{\mathrm{T}}+\int\frac{\partial\Phi^{(l,c)}}{\partial z}\mathrm{d}z\mathbf{P}_c^{\mathrm{T}}\right)\begin{bmatrix}\delta\varepsilon_{xx}^{(l,0)}\\\delta\varepsilon_{yy}^{(l,0)}\\\delta\varepsilon_{xy}^{(l,0)}\end{bmatrix}+\left(\begin{bmatrix}u_1^{(c)}\\u_2^{(c)}\\u_3\end{bmatrix}^{\mathrm{T}}\mathbf{M}_c^{\mathrm{T}}+\int Z\frac{\partial\Phi^{(l,c)}}{\partial z}\mathrm{d}z\mathbf{P}_c^{\mathrm{T}}\right)\begin{bmatrix}\delta\varepsilon_{xx}^{(l,1)}\\\delta\varepsilon_{yy}^{(l,1)}\\\delta\varepsilon_{xy}^{(l,1)}\end{bmatrix}, \quad (20)$$

where

$$\mathbf{N}_c^{\mathrm{T}}=\mathbf{J}_0^{\mathrm{T}}\mathbf{A}^{(c)}+\mathbf{J}_1^{\mathrm{T}}\mathbf{B}^{(c)},\mathbf{M}_c^{\mathrm{T}}=\mathbf{J}_0^{\mathrm{T}}\mathbf{B}^{(c)}+\mathbf{J}_1^{\mathrm{T}}\mathbf{D}^{(c)},\mathbf{P}_c^{\mathrm{T}}=\begin{bmatrix}\bar{e}_{31}^{(l,c)} & \bar{e}_{32}^{(l,c)} & \bar{e}_{36}^{(l,c)}\end{bmatrix}. \quad (21)$$

The elements of the reduced stiffness matrices $\mathbf{A}^{(c)}$, $\mathbf{B}^{(c)}$ and $\mathbf{D}^{(c)}$ for the constraining plate are expressed as

$$A_{ij}^{(c)}=\sum_{l=1}^{N}\bar{Q}_{ij}^{(l,c)}\left(h_l-h_{l-1}\right),B_{ij}^{(c)}=\frac{1}{2}\sum_{l=1}^{N}\bar{Q}_{ij}^{(l,c)}\left(h_l^2-h_{l-1}^2\right),D_{ij}^{(c)}=\frac{1}{3}\sum_{l=1}^{N}\bar{Q}_{ij}^{(l,c)}\left(h_l^3-h_{l-1}^3\right), \quad (22)$$

where h_l is the local Z coordinate of the top plane for the $l-$th lamina. Reduced stiffnesses $\bar{Q}_{ij}^{(l,c)}$ of the $l-$th orthotropic layer for the constraining plate are defined by

$$\bar{Q}_{11}^{(l,c)}=Q_{11}^{(l,c)}\cos^4\alpha+2\left(Q_{12}^{(l,c)}+2Q_{66}^{(l,c)}\right)\sin^2\alpha\cos^2\alpha+Q_{22}^{(l,c)}\sin^4\alpha,$$
$$\bar{Q}_{12}^{(l,c)}=Q_{12}^{(l,c)}+\left(Q_{11}^{(l,c)}+Q_{22}^{(l,c)}-2Q_{12}^{(l,c)}-4Q_{66}^{(l,c)}\right)\sin^2\alpha\cos^2\alpha,$$
$$\bar{Q}_{22}^{(l,c)}=Q_{22}^{(l,c)}\cos^4\alpha+2\left(Q_{12}^{(l,c)}+2Q_{66}^{(l,c)}\right)\sin^2\alpha\cos^2\alpha+Q_{11}^{(l,c)}\sin^4\alpha,$$
$$\bar{Q}_{66}^{(l,c)}=Q_{66}^{(l,c)}+\left(Q_{11}^{(l,c)}+Q_{22}^{(l,c)}-2Q_{12}^{(l,c)}-4Q_{66}^{(l,c)}\right)\sin^2\alpha\cos^2\alpha,$$

$$\bar{Q}_{16}^{(l,c)} = \left(Q_{11}^{(l,c)} - Q_{12}^{(l,c)} - 2Q_{66}^{(l,c)}\right)\sin\alpha\cos^3\alpha - \left(Q_{22}^{(l,c)} - Q_{12}^{(l,c)} - 2Q_{66}^{(l,c)}\right)\sin^3\alpha\cos\alpha,$$
$$\bar{Q}_{26}^{(l,c)} = \left(Q_{11}^{(l,c)} - Q_{12}^{(l,c)} - 2Q_{66}^{(l,c)}\right)\sin^3\alpha\cos\alpha - \left(Q_{22}^{(l,c)} - Q_{12}^{(l,c)} - 2Q_{66}^{(l,c)}\right)\sin\alpha\cos^3\alpha, \quad (23)$$

where α is the fibre orientation angle of the lamina. The reduced piezoelectric coefficients $\bar{e}_{ij}^{(l,c)}$ and permittivity coefficients $\bar{\xi}_{ij}^{(l,c)}$ of the $l-$th orthotropic layer are given by

$$\bar{e}_{31}^{(l,c)} = e_{31}^{(l,c)}\cos^2\alpha + e_{32}^{(l,c)}\sin^2\alpha, \bar{e}_{32}^{(l,c)} = e_{31}^{(l,c)}\sin^2\alpha + e_{32}^{(l,c)}\cos^2\alpha,$$
$$\bar{e}_{36}^{(l,c)} = \left(e_{31}^{(l,c)} - e_{32}^{(l,c)}\right)\sin\alpha\cos\alpha, \bar{\xi}_{11}^{(l,c)} = \xi_{11}^{(l,c)}\cos^2\alpha + \xi_{22}^{(l,c)}\sin^2\alpha,$$
$$\bar{\xi}_{22}^{(l,c)} = \xi_{11}^{(l,c)}\sin^2\alpha + \xi_{22}^{(l,c)}\cos^2\alpha, \bar{\xi}_{12}^{(l,c)} = \left(\xi_{11}^{(l,c)} - \xi_{22}^{(l,c)}\right)\sin\alpha\cos\alpha, \bar{\xi}_{33}^{(l,c)} = \xi_{33}^{(l,c)}. \quad (24)$$

The differential operator matrices $\mathbf{J}_0$ and $\mathbf{J}_1$ are defined as

$$\mathbf{J}_0 = \begin{bmatrix} \frac{\partial}{\partial x} & 0 & 0 \\ 0 & \frac{\partial}{\partial y} & 0 \\ \frac{\partial}{\partial y} & \frac{\partial}{\partial x} & 0 \end{bmatrix}, \mathbf{J}_1 = \begin{bmatrix} 0 & 0 & -\frac{\partial^2}{\partial x^2} \\ 0 & 0 & -\frac{\partial^2}{\partial y^2} \\ 0 & 0 & -2\frac{\partial^2}{\partial x \partial y} \end{bmatrix}. \quad (25)$$

According to Eqs. (10) and (13), one obtains

$$\begin{bmatrix} \delta\varepsilon_{xx}^{(l,0)} & \delta\varepsilon_{yy}^{(l,0)} & \delta\varepsilon_{xy}^{(l,0)} \end{bmatrix}^{\mathrm{T}} = \delta\left(\mathbf{J}_0\begin{bmatrix} u_1^{(c)} & u_2^{(c)} & u_3 \end{bmatrix}^{\mathrm{T}}\right) = -\mathbf{J}_0\begin{bmatrix} \delta u_1^{(c)} & \delta u_2^{(c)} & \delta u_3 \end{bmatrix}^{\mathrm{T}} \quad (26)$$

$$\begin{bmatrix} \delta\varepsilon_{xx}^{(l,1)} & \delta\varepsilon_{yy}^{(l,1)} & \delta\varepsilon_{xy}^{(l,1)} \end{bmatrix}^{\mathrm{T}} = \delta\left(\mathbf{J}_1\begin{bmatrix} u_1^{(c)} & u_2^{(c)} & u_3 \end{bmatrix}^{\mathrm{T}}\right) = \mathbf{J}_1\begin{bmatrix} \delta u_1^{(c)} & \delta u_2^{(c)} & \delta u_3 \end{bmatrix}^{\mathrm{T}}, \quad (27)$$

$$\delta\left(\mathbf{E}_l^{(c)}\right)^{\mathrm{T}} = -\delta\begin{bmatrix} \frac{\partial\Phi^{(l,c)}}{\partial x} & \frac{\partial\Phi^{(l,c)}}{\partial y} & \frac{\partial\Phi^{(l,c)}}{\partial z} \end{bmatrix}. \quad (28)$$

Substituting Eqs. (26) and (27) into Eq. (20), one obtains

$$\begin{aligned} &\int_z \delta\left(\boldsymbol{\varepsilon}_l^{(c)}\right)^{\mathrm{T}}\left(\mathbf{Q}_l^{(c)}\boldsymbol{\varepsilon}_l^{(c)} - \mathbf{e}_l^{(c)}\mathbf{E}_l^{(c)}\right)\mathrm{d}z \\ &= -\left(\begin{bmatrix} u_1^{(c)} & u_2^{(c)} & u_3 \end{bmatrix}\left(\mathbf{J}_0^{\mathrm{T}}\mathbf{A}^{(c)} + \mathbf{J}_1^{\mathrm{T}}\mathbf{B}^{(c)}\right) + \int\frac{\partial\Phi^{(l,c)}}{\partial z}\mathrm{d}z\mathbf{P}_c^{\mathrm{T}}\right)\mathbf{J}_0\begin{bmatrix} \delta u_1^{(c)} & \delta u_2^{(c)} & \delta u_3 \end{bmatrix}^{\mathrm{T}} \\ &+\left(\begin{bmatrix} u_1^{(c)} & u_2^{(c)} & u_3 \end{bmatrix}\left(\mathbf{J}_0^{\mathrm{T}}\mathbf{B}^{(c)} + \mathbf{J}_1^{\mathrm{T}}\mathbf{D}^{(c)}\right) + \int Z\frac{\partial\Phi^{(l,c)}}{\partial z}\mathrm{d}z\mathbf{P}_c^{\mathrm{T}}\right)\mathbf{J}_1\begin{bmatrix} \delta u_1^{(c)} & \delta u_2^{(c)} & \delta u_3 \end{bmatrix}^{\mathrm{T}} \quad (29) \end{aligned}$$

Similarly, simplifying the third term on the left-hand side in Eq. (19), one obtains

$$\int_z \delta\left(\boldsymbol{\varepsilon}_l^{(s)}\right)^{\mathrm{T}}\left(\mathbf{Q}_l^{(s)}\boldsymbol{\varepsilon}_l^{(s)} - \mathbf{e}_l^{(s)}\mathbf{E}_l^{(s)}\right)\mathrm{d}z$$

$$= \left(\begin{bmatrix} u_1^{(s)} \\ u_2^{(s)} \\ u_3 \end{bmatrix}^{\mathrm{T}} \mathbf{N}_s^{\mathrm{T}} + \int \frac{\partial \Phi^{(l,s)}}{\partial z} \mathrm{d}z \mathbf{P}_s^{\mathrm{T}} \right) \begin{bmatrix} \delta\varepsilon_{xx}^{(l,0)} \\ \delta\varepsilon_{yy}^{(l,0)} \\ \delta\varepsilon_{xy}^{(l,0)} \end{bmatrix} + \left(\begin{bmatrix} u_1^{(s)} \\ u_2^{(s)} \\ u_3 \end{bmatrix}^{\mathrm{T}} \mathbf{M}_s^{\mathrm{T}} + \int Z \frac{\partial \Phi^{(l,s)}}{\partial z} \mathrm{d}z \mathbf{P}_s^{\mathrm{T}} \right) \begin{bmatrix} \delta\varepsilon_{xx}^{(l,1)} \\ \delta\varepsilon_{yy}^{(l,1)} \\ \delta\varepsilon_{xy}^{(l,1)} \end{bmatrix}, \tag{30}$$

where

$$\begin{bmatrix} \mathbf{N}_s^{\mathrm{T}} & \mathbf{M}_s^{\mathrm{T}} \end{bmatrix} = \begin{bmatrix} \mathbf{J}_0^{\mathrm{T}} \mathbf{A}^{(s)} + \mathbf{J}_1^{\mathrm{T}} \mathbf{B}^{(s)} & \mathbf{J}_0^{\mathrm{T}} \mathbf{B}^{(s)} + \mathbf{J}_1^{\mathrm{T}} \mathbf{D}^{(s)} \end{bmatrix}, \mathbf{P}_s^{\mathrm{T}} = \begin{bmatrix} \bar{e}_{31}^{(l,s)} & \bar{e}_{32}^{(l,s)} & \bar{e}_{36}^{(l,s)} \end{bmatrix}. \tag{31}$$

The elements of the reduced stiffness matrices $\mathbf{A}^{(s)}$, $\mathbf{B}^{(s)}$ and $\mathbf{D}^{(s)}$ for the host plate are expressed as

$$A_{ij}^{(s)} = \sum_{l=1}^{N} \bar{Q}_{ij}^{(l,s)} (h_l - h_{l-1}), B_{ij}^{(s)} = \frac{1}{2} \sum_{l=1}^{N} \bar{Q}_{ij}^{(l,s)} \left(h_l^2 - h_{l-1}^2 \right), D_{ij}^{(s)} = \frac{1}{3} \sum_{l=1}^{N} \bar{Q}_{ij}^{(l,s)} \left(h_l^3 - h_{l-1}^3 \right). \tag{32}$$

The governing equations of the constrained composite plate with double piezoelectric layers can be obtained by simplifying Eq. (19), which derives seven equations of motion for the composite plate shown in Fig. 1. It is necessary to further simplify the seven integral-differential hybird equations which are difficult to solve. The following derivations are required to find the solutions to the electric potential equations expressed by $\tilde{u}_1^{(c)}$, $\tilde{u}_2^{(c)}$, $\tilde{u}_1^{(s)}$, $\tilde{u}_2^{(s)}$ and $\tilde{u}_3$ in order to get the simplified governing equations.

2.1.1.4 Solution to the electric potential equations According to Eq. (19), one obtains the electric potential equation of the constraining plate with a single smart layer

$$\begin{aligned} &-\bar{e}_{31}^{(l,c)} \frac{\partial^2 u_3}{\partial x^2} - \bar{e}_{32}^{(l,c)} \frac{\partial^2 u_3}{\partial y^2} - 2\bar{e}_{36}^{(l,c)} \frac{\partial^2 u_3}{\partial x \partial y} \\ &-\left(\bar{\xi}_{11}^{(l,c)} \frac{\partial^2 \Phi^{(l,c)}}{\partial x^2} + 2\bar{\xi}_{12}^{(l,c)} \frac{\partial^2 \Phi^{(l,c)}}{\partial x \partial y} + \bar{\xi}_{22}^{(l,c)} \frac{\partial^2 \Phi^{(l,c)}}{\partial y^2} + \bar{\xi}_{33}^{(l,c)} \frac{\partial^2 \Phi^{(l,c)}}{\partial z^2} \right) = 0. \end{aligned} \tag{33}$$

Similarly, the electric potential equation of the host plate with a single smart layer is described by

$$\begin{aligned} &-\bar{e}_{31}^{(l,s)} \frac{\partial^2 u_3}{\partial x^2} - \bar{e}_{32}^{(l,s)} \frac{\partial^2 u_3}{\partial y^2} - 2\bar{e}_{36}^{(l,s)} \frac{\partial^2 u_3}{\partial x \partial y} \\ &-\left(\bar{\xi}_{11}^{(l,s)} \frac{\partial^2 \Phi^{(l,s)}}{\partial x^2} + 2\bar{\xi}_{12}^{(l,s)} \frac{\partial^2 \Phi^{(l,s)}}{\partial x \partial y} + \bar{\xi}_{22}^{(l,s)} \frac{\partial^2 \Phi^{(l,s)}}{\partial y^2} + \bar{\xi}_{33}^{(l,s)} \frac{\partial^2 \Phi^{(l,s)}}{\partial z^2} \right) = 0. \end{aligned} \tag{34}$$

According to Eq. (12), one obtains the electric displacement $D_3^{(l,c)}$ of the constraining plate

$$
\begin{aligned}
D_3^{(l,c)}\Big|_{Z=h_{p_c}} &= \bar{e}_{31}^{(l,c)}\frac{\partial u_1^{(c)}}{\partial x} + \bar{e}_{36}^{(l,c)}\frac{\partial u_1^{(c)}}{\partial y} + \bar{e}_{32}^{(l,c)}\frac{\partial u_2^{(c)}}{\partial y} + \bar{e}_{36}^{(l,c)}\frac{\partial u_2^{(c)}}{\partial x} \\
&-h_{p_c}\bar{e}_{31}^{(l,c)}\frac{\partial^2 u_3}{\partial x^2} - h_{p_c}\bar{e}_{32}^{(l,c)}\frac{\partial^2 u_3}{\partial y^2} - 2h_{p_c}\bar{e}_{36}^{(l,c)}\frac{\partial^2 u_3}{\partial x \partial y} - \bar{\xi}_{33}^{(l,c)}\frac{\partial \Phi^{(l,c)}}{\partial z},
\end{aligned} \tag{35}
$$

where h_{p_c} is the local Z coordinate of the piezoelectric layer in the constraining plate. Similarly, one obtains the electric displacement $D_3^{(l,s)}$ of the host plate

$$
\begin{aligned}
D_3^{(l,s)}\Big|_{Z=h_{p_s}} &= \bar{e}_{31}^{(l,s)}\frac{\partial u_1^{(s)}}{\partial x} + \bar{e}_{36}^{(l,s)}\frac{\partial u_1^{(s)}}{\partial y} + \bar{e}_{32}^{(l,s)}\frac{\partial u_2^{(s)}}{\partial y} + \bar{e}_{36}^{(l,s)}\frac{\partial u_2^{(s)}}{\partial x} \\
&-h_{p_s}\bar{e}_{31}^{(l,s)}\frac{\partial^2 u_3}{\partial x^2} - h_{p_s}\bar{e}_{32}^{(l,s)}\frac{\partial^2 u_3}{\partial y^2} - 2h_{p_s}\bar{e}_{36}^{(l,s)}\frac{\partial^2 u_3}{\partial x \partial y} - \bar{\xi}_{33}^{(l,s)}\frac{\partial \Phi^{(l,s)}}{\partial z},
\end{aligned} \tag{36}
$$

where h_{p_s} is the local Z coordinate of the piezoelectric layer in the host plate. The two-dimensional Fourier transform and inverse Fourier transform are defined by

$$
\begin{aligned}
\tilde{f}\left(k_x, k_y\right) &= \int_{-\infty}^{+\infty}\int_{-\infty}^{+\infty} f\left(x, y\right) \mathrm{e}^{-\mathrm{i}k_x x}\mathrm{e}^{-\mathrm{i}k_y y}\mathrm{d}x\mathrm{d}y, \\
f\left(x, y\right) &= \frac{1}{4\pi^2}\int_{-\infty}^{+\infty}\int_{-\infty}^{+\infty} \tilde{f}\left(k_x, k_y\right) \mathrm{e}^{\mathrm{i}k_x x}\mathrm{e}^{\mathrm{i}k_y y}\mathrm{d}k_x\mathrm{d}k_y.
\end{aligned} \tag{37}
$$

Taking the Fourier transform with respect to Eq. (33), one obtains the solution in the wavenumber domain

$$
\tilde{\Phi}^{(l,c)} = -\frac{\bar{e}_{31}^{(l,c)}k_x^2 + \bar{e}_{32}^{(l,c)}k_y^2 + 2\bar{e}_{36}^{(l,c)}k_x k_y}{\bar{\xi}_{11}^{(l,c)}k_x^2 + 2\bar{\xi}_{12}^{(l,c)}k_x k_y + \bar{\xi}_{22}^{(l,c)}k_y^2}\tilde{u}_3 + c_1\mathrm{e}^{k_{p1}^{(c)}z} + c_2\mathrm{e}^{k_{p2}^{(c)}z}, \tag{38}
$$

where c_1 and c_2 are the coefficients of the electric potential for the constraining plate. $k_{p1}^{(c)}$ and $k_{p2}^{(c)}$ are given by

$$
\begin{aligned}
k_{p1}^{(c)} &= \left(\frac{\bar{\xi}_{11}^{(l,c)}k_x^2 + 2\bar{\xi}_{12}^{(l,c)}k_x k_y + \bar{\xi}_{22}^{(l,c)}k_y^2}{\bar{\xi}_{33}^{(l,c)}}\right)^{1/2}, \\
k_{p2}^{(c)} &= -\left(\frac{\bar{\xi}_{11}^{(l,c)}k_x^2 + 2\bar{\xi}_{12}^{(l,c)}k_x k_y + \bar{\xi}_{22}^{(l,c)}k_y^2}{\bar{\xi}_{33}^{(l,c)}}\right)^{1/2}.
\end{aligned} \tag{39}
$$

Similarly, the solution to Eq. (34) in the wavenumber domain is described by

$$
\tilde{\Phi}^{(l,s)} = -\frac{\bar{e}_{31}^{(l,s)}k_x^2 + \bar{e}_{32}^{(l,s)}k_y^2 + 2\bar{e}_{36}^{(l,s)}k_x k_y}{\bar{\xi}_{11}^{(l,s)}k_x^2 + 2\bar{\xi}_{12}^{(l,s)}k_x k_y + \bar{\xi}_{22}^{(l,s)}k_y^2}\tilde{u}_3 + c_3\mathrm{e}^{k_{p1}^{(s)}z} + c_4\mathrm{e}^{k_{p2}^{(s)}z}, \tag{40}
$$

where c_3 and c_4 are the coefficients of the electric potential for the host plate. c_1, c_2, c_3 and c_4 are determined by the electric boundary conditions. $k_{p1}^{(s)}$ and $k_{p2}^{(s)}$ are given by

$$k_{p1}^{(s)} = \left(\frac{\bar{\xi}_{11}^{(l,s)} k_x^2 + 2\bar{\xi}_{12}^{(l,s)} k_x k_y + \bar{\xi}_{22}^{(l,s)} k_y^2}{\bar{\xi}_{33}^{(l,s)}} \right)^{1/2},$$
$$k_{p2}^{(s)} = -\left(\frac{\bar{\xi}_{11}^{(l,s)} k_x^2 + 2\bar{\xi}_{12}^{(l,s)} k_x k_y + \bar{\xi}_{22}^{(l,s)} k_y^2}{\bar{\xi}_{33}^{(l,s)}} \right)^{1/2}. \tag{41}$$

According to Eqs. (38) and (40), one obtains

$$\int_{h_{c1}}^{h_{c2}} \frac{\partial \tilde{\Phi}^{(l,c)}}{\partial z} \mathrm{d}Z = \begin{bmatrix} c_1 & c_2 \end{bmatrix} \begin{bmatrix} \mathrm{e}^{k_{p1}^{(c)} h_{c_2}} - \mathrm{e}^{k_{p1}^{(c)} h_{c_1}} \\ \mathrm{e}^{k_{p2}^{(c)} h_{c_2}} - \mathrm{e}^{k_{p2}^{(c)} h_{c_1}} \end{bmatrix}, \int_{h_{s1}}^{h_{s2}} \frac{\partial \tilde{\Phi}^{(l,s)}}{\partial z} \mathrm{d}Z = \begin{bmatrix} c_3 & c_4 \end{bmatrix} \begin{bmatrix} \mathrm{e}^{k_{p1}^{(s)} h_{s_2}} - \mathrm{e}^{k_{p1}^{(s)} h_{s_1}} \\ \mathrm{e}^{k_{p2}^{(s)} h_{s_2}} - \mathrm{e}^{k_{p2}^{(s)} h_{s_1}} \end{bmatrix}, \tag{42}$$

$$\int_{h_{c1}}^{h_{c2}} Z \frac{\partial \tilde{\Phi}^{(l,c)}}{\partial z} \mathrm{d}Z = \begin{bmatrix} c_1 & c_2 \end{bmatrix} \begin{bmatrix} h_{c2} \mathrm{e}^{k_{p1}^{(c)} h_{c_2}} - \frac{\mathrm{e}^{k_{p1}^{(c)} h_{c_2}}}{k_{p1}^{(c)}} - h_{c1} \mathrm{e}^{k_{p1}^{(c)} h_{c_1}} + \frac{\mathrm{e}^{k_{p1}^{(c)} h_{c_1}}}{k_{p1}^{(c)}} \\ h_{c2} \mathrm{e}^{k_{p2}^{(c)} h_{c_2}} - \frac{\mathrm{e}^{k_{p2}^{(c)} h_{c_2}}}{k_{p2}^{(c)}} - h_{c1} \mathrm{e}^{k_{p2}^{(c)} h_{c_1}} + \frac{\mathrm{e}^{k_{p2}^{(c)} h_{c_1}}}{k_{p2}^{(c)}} \end{bmatrix}, \tag{43}$$

$$\int_{h_{s1}}^{h_{s2}} Z \frac{\partial \tilde{\Phi}^{(l,s)}}{\partial z} \mathrm{d}Z = \begin{bmatrix} c_3 & c_4 \end{bmatrix} \begin{bmatrix} h_{s2} \mathrm{e}^{k_{p1}^{(s)} h_{s2}} - \frac{\mathrm{e}^{k_{p1}^{(s)} h_{s2}}}{k_{p1}^{(s)}} - h_{s1} \mathrm{e}^{k_{p1}^{(s)} h_{s1}} + \frac{\mathrm{e}^{k_{p1}^{(s)} h_{s1}}}{k_{p1}^{(s)}} \\ h_{s2} \mathrm{e}^{k_{p2}^{(s)} h_{s_2}} - \frac{\mathrm{e}^{k_{p2}^{(s)} h_{s2}}}{k_{p2}^{(s)}} - h_{s1} \mathrm{e}^{k_{p2}^{(s)} h_{s_1}} + \frac{\mathrm{e}^{k_{p2}^{(s)} h_{s1}}}{k_{p2}^{(s)}} \end{bmatrix}. \tag{44}$$

where h_{c_1} and h_{c_2} are the local Z coordinates of the lower and upper surfaces for the piezoelectric layer of the constraining plate, respectively. h_{s_1} and h_{s_2} are the local Z coordinates of the lower and upper surfaces for the piezoelectric layer of the host plate, respectively.

2.1.2 Double piezoelectric layers with closed circuit boundary conditions

Electric boundary conditions of two piezoelectric layers with closed circuit connection are described by

$$\Phi^{(l,c)}\big|_{Z=h_{c_1}} = 0,\ \Phi^{(l,c)}\big|_{Z=h_{c_2}} = 0,\ \Phi^{(l,s)}\big|_{Z=h_{s_1}} = 0,\ \Phi^{(l,s)}\big|_{Z=h_{s_2}} = 0. \tag{45}$$

Substituting Eqs. (38) and (40) into Eq. (45) with the Fourier transform, one obtains

$$\begin{bmatrix} c_1 \\ c_2 \end{bmatrix} = \begin{bmatrix} \mathrm{e}^{k_{p1}^{(c)} h_{c_1}} & \mathrm{e}^{k_{p2}^{(c)} h_{c_1}} \\ \mathrm{e}^{k_{p1}^{(c)} h_{c_2}} & \mathrm{e}^{k_{p2}^{(c)} h_{c_2}} \end{bmatrix}^{-1} \begin{bmatrix} 1 \\ 1 \end{bmatrix} \frac{\bar{e}_{31}^{(k,c)} k_x^2 + \bar{e}_{32}^{(k,c)} k_y^2 + 2\bar{e}_{36}^{(k,c)} k_x k_y}{\bar{\xi}_{11}^{(k,c)} k_x^2 + 2\bar{\xi}_{12}^{(k,c)} k_x k_y + \bar{\xi}_{22}^{(k,c)} k_y^2} \tilde{u}_3, \tag{46}$$

$$\begin{bmatrix} c_3 \\ c_4 \end{bmatrix} = \begin{bmatrix} \mathrm{e}^{k_{p1}^{(s)} h_{s_1}} & \mathrm{e}^{k_{p2}^{(s)} h_{s_1}} \\ \mathrm{e}^{k_{p1}^{(s)} h_{s_2}} & \mathrm{e}^{k_{p2}^{(s)} h_{s_2}} \end{bmatrix}^{-1} \begin{bmatrix} 1 \\ 1 \end{bmatrix} \frac{\bar{e}_{31}^{(k,s)} k_x^2 + \bar{e}_{32}^{(k,s)} k_y^2 + 2\bar{e}_{36}^{(k,s)} k_x k_y}{\bar{\xi}_{11}^{(k,s)} k_x^2 + 2\bar{\xi}_{12}^{(k,s)} k_x k_y + \bar{\xi}_{22}^{(k,s)} k_y^2} \tilde{u}_3. \tag{47}$$

Thus, the electric potentials in the two piezoelectric layers are expressed by the transverse displacement spectra $\tilde{u}_3$.

2.1.3 Double piezoelectric layers with open circuit boundary conditions

Electric boundary conditions of two piezoelectric layers with open circuit connection are described by

$$D_3^{(l,c)}\Big|_{Z=h_{c_1}} = 0,\ D_3^{(l,c)}\Big|_{Z=h_{c_2}} = 0,\ D_3^{(l,s)}\Big|_{Z=h_{s_1}} = 0,\ D_3^{(l,s)}\Big|_{Z=h_{s_2}} = 0. \tag{48}$$

Similarly, substituting Eqs. (35), (36), (38) and (40) into Eq. (48) with the Fourier transform, one obtains

$$\begin{bmatrix} c_1 \\ c_2 \end{bmatrix} = \begin{bmatrix} \bar{\xi}_{33}^{(l,c)} k_{p1}^{(c)} \mathrm{e}^{k_{p1}^{(c)} h_{c_1}} & \bar{\xi}_{33}^{(l,c)} k_{p2}^{(c)} \mathrm{e}^{k_{p2}^{(c)} h_{c_1}} \\ \bar{\xi}_{33}^{(l,c)} k_{p1}^{(c)} \mathrm{e}^{k_{p1}^{(c)} h_{c_2}} & \bar{\xi}_{33}^{(l,c)} k_{p2}^{(c)} \mathrm{e}^{k_{p2}^{(c)} h_{c_2}} \end{bmatrix}^{-1}$$

$$\begin{bmatrix} \bar{e}_{31}^{(l,c)} \mathrm{i}k_x + \bar{e}_{36}^{(l,c)} \mathrm{i}k_y & \bar{e}_{32}^{(l,c)} \mathrm{i}k_y + \bar{e}_{36}^{(l,c)} \mathrm{i}k_x & h_{c_1} \bar{e}_{31}^{(l,c)} k_x^2 + h_{c_1} \bar{e}_{32}^{(l,c)} k_y^2 + 2h_{c_1} \bar{e}_{36}^{(l,c)} k_x k_y \\ \bar{e}_{31}^{(l,c)} \mathrm{i}k_x + \bar{e}_{36}^{(l,c)} \mathrm{i}k_y & \bar{e}_{32}^{(l,c)} \mathrm{i}k_y + \bar{e}_{36}^{(l,c)} \mathrm{i}k_x & h_{c_2} \bar{e}_{31}^{(l,c)} k_x^2 + h_{c_2} \bar{e}_{32}^{(l,c)} k_y^2 + 2h_{c_2} \bar{e}_{36}^{(l,c)} k_x k_y \end{bmatrix} \begin{bmatrix} \tilde{u}_1^{(c)} \\ \tilde{u}_2^{(c)} \\ \tilde{u}_3 \end{bmatrix}, \tag{49}$$

$$\begin{bmatrix} c_3 \\ c_4 \end{bmatrix} = \begin{bmatrix} \bar{\xi}_{33}^{(l,s)} k_{p1}^{(s)} \mathrm{e}^{k_{p1}^{(s)} h_{s_1}} & \bar{\xi}_{33}^{(l,s)} k_{p2}^{(s)} \mathrm{e}^{k_{p2}^{(s)} h_{s_1}} \\ \bar{\xi}_{33}^{(l,s)} k_{p1}^{(s)} \mathrm{e}^{k_{p1}^{(s)} h_{s_2}} & \bar{\xi}_{33}^{(l,s)} k_{p2}^{(s)} \mathrm{e}^{k_{p2}^{(s)} h_{s_2}} \end{bmatrix}^{-1}$$

$$\begin{bmatrix} \bar{e}_{31}^{(l,s)} \mathrm{i}k_x + \bar{e}_{36}^{(l,s)} \mathrm{i}k_y & \bar{e}_{32}^{(l,s)} \mathrm{i}k_y + \bar{e}_{36}^{(l,s)} \mathrm{i}k_x & h_{s_1} \bar{e}_{31}^{(l,s)} k_x^2 + h_{s_1} \bar{e}_{32}^{(l,s)} k_y^2 + 2h_{s_1} \bar{e}_{36}^{(l,s)} k_x k_y \\ \bar{e}_{31}^{(l,s)} \mathrm{i}k_x + \bar{e}_{36}^{(l,s)} \mathrm{i}k_y & \bar{e}_{32}^{(l,s)} \mathrm{i}k_y + \bar{e}_{36}^{(l,s)} \mathrm{i}k_x & h_{s_2} \bar{e}_{31}^{(l,s)} k_x^2 + h_{s_2} \bar{e}_{32}^{(l,s)} k_y^2 + 2h_{s_2} \bar{e}_{36}^{(l,s)} k_x k_y \end{bmatrix} \begin{bmatrix} \tilde{u}_1^{(s)} \\ \tilde{u}_2^{(s)} \\ \tilde{u}_3 \end{bmatrix}. \tag{50}$$

Thus, the electric potentials in the two piezoelectric layers are determined by the displacement spectra of composite plates.

2.1.4 Double piezoelectric layers connected by a dielectric slab with uniform resistances and inductances

Double piezoelectric layers are connected by a dielectric slab with uniform resistances and inductances which are used to dissipate electric energy. Electric boundary conditions are given by

$$\Phi^{(l,c)}\Big|_{Z=h_{c_2}} - \Phi^{(l,s)}\Big|_{Z=h_{s_1}} = (R - \mathrm{i}\omega L)\,\frac{\mathrm{d}q}{\mathrm{d}t}, \mathrm{d}q = D_3^{(l,c)}\Big|_{Z=h_{c_2}} \Delta S, \tag{51}$$

$$D_3^{(l,s)}\Big|_{Z=h_{s_1}} = D_3^{(l,c)}\Big|_{Z=h_{c_2}}, \Phi^{(l,c)}\Big|_{Z=h_{c_1}} = 0, \Phi^{(l,s)}\Big|_{Z=h_{s_2}} = 0, \tag{52}$$

where R and L are the distributed resistances and inductances of the dielectric slab. ΔS and q are the infinitesimal area and the induced charges of the piezoelectric layers. Introducing the resistance coefficient ρ_R and inductance coefficient C_L, one obtains

$$R = C_R/\Delta S, L = C_L/\Delta S, C_R = l_r\rho_R, \tag{53}$$

where l_r is the thickness of the external dielectric slab. Substituting Eq. (53) into Eq. (51), one obtains

$$\Phi^{(l,c)}\Big|_{Z=h_{c_2}} - \Phi^{(l,s)}\Big|_{Z=h_{s_1}} = -\mathrm{i}\omega\,(C_R - \mathrm{i}\omega C_L)\,D_3^{(l,c)}\Big|_{Z=h_{c_2}}, \tag{54}$$

Substituting Eqs. (35), (36), (38) and (40) into Eqs. (52) and (54) with the Fourier transform, one obtains

$$\begin{bmatrix} c_1 & c_2 & c_3 & c_4 \end{bmatrix}^{\mathrm{T}} = \mathbf{G}^{-1}\mathbf{E}\begin{bmatrix} \tilde{u}_1^{(s)} & \tilde{u}_2^{(s)} & \tilde{u}_3 & \tilde{u}_1^{(c)} & \tilde{u}_2^{(c)} \end{bmatrix}^{\mathrm{T}}, \tag{55}$$

where the elements G_{ij} of the matrix $\mathbf{G}$ are given by

$$\begin{aligned}
&G_{11} = \bar{\xi}_{33}^{(l,c)}k_{p1}^{(c)}\mathrm{e}^{k_{p1}^{(c)}h_{c_2}}, G_{12} = \bar{\xi}_{33}^{(l,c)}k_{p2}^{(c)}\mathrm{e}^{k_{p2}^{(c)}h_{c_2}}, G_{13} = -\bar{\xi}_{33}^{(l,s)}k_{p1}^{(s)}\mathrm{e}^{k_{p1}^{(s)}h_{s_1}}, G_{14} = -\bar{\xi}_{33}^{(l,s)}k_{p2}^{(s)}\mathrm{e}^{k_{p2}^{(s)}h_{s_1}},\\
&G_{21} = \mathrm{e}^{k_{p1}^{(c)}h_{c_1}}, G_{22} = \mathrm{e}^{k_{p2}^{(c)}h_{c_1}}, G_{23} = 0, G_{24} = 0, G_{31} = 0, G_{32} = 0, G_{33} = \mathrm{e}^{k_{p1}^{(s)}h_{s_2}}, G_{34} = \mathrm{e}^{k_{p2}^{(s)}h_{s_2}},\\
&G_{41} = \mathrm{e}^{k_{p1}^{(c)}h_{c_2}} - \left(\mathrm{i}\omega C_R + \omega^2 C_L\right)\bar{\xi}_{33}^{(l,c)}k_{p1}^{(c)}\mathrm{e}^{k_{p1}^{(c)}h_{c_2}},\\
&G_{42} = \mathrm{e}^{k_{p2}^{(c)}h_{c_2}} - \left(\mathrm{i}\omega C_R + \omega^2 C_L\right)\bar{\xi}_{33}^{(l,c)}k_{p2}^{(c)}\mathrm{e}^{k_{p2}^{(c)}h_{c_2}}, G_{43} = -\mathrm{e}^{k_{p1}^{(s)}h_{s_1}}, G_{44} = -\mathrm{e}^{k_{p2}^{(s)}h_{s_1}},
\end{aligned} \tag{56}$$

the elements E_{ij} of the matrix $\mathbf{E}$ are given by

$$
\begin{aligned}
&E_{11} = -\bar{e}_{31}^{(l,s)}\mathrm{i}k_x - \bar{e}_{36}^{(l,s)}\mathrm{i}k_y, E_{12} = -\bar{e}_{32}^{(l,s)}\mathrm{i}k_y - \bar{e}_{36}^{(l,s)}\mathrm{i}k_x,\\
&E_{13} = \left(h_{c_2}\bar{e}_{31}^{(l,c)} - h_{s_1}\bar{e}_{31}^{(l,s)}\right)k_x^2 + \left(h_{c_2}\bar{e}_{32}^{(l,c)} - h_{s_1}\bar{e}_{32}^{(l,s)}\right)k_y^2 + 2\left(h_{c_2}\bar{e}_{36}^{(l,c)} - h_{s_1}\bar{e}_{36}^{(l,s)}\right)k_xk_y,\\
&E_{14} = \bar{e}_{31}^{(l,c)}\mathrm{i}k_x + \bar{e}_{36}^{(l,c)}\mathrm{i}k_y, E_{15} = \bar{e}_{32}^{(l,c)}\mathrm{i}k_y + \bar{e}_{36}^{(l,c)}\mathrm{i}k_x,\\
&E_{21} = 0, E_{22} = 0, E_{23} = \frac{\bar{e}_{31}^{(l,c)}k_x^2 + \bar{e}_{32}^{(l,c)}k_y^2 + 2\bar{e}_{36}^{(l,c)}k_xk_y}{\bar{\xi}_{11}^{(l,c)}k_x^2 + 2\bar{\xi}_{12}^{(l,c)}k_xk_y + \bar{\xi}_{22}^{(l,c)}k_y^2}, E_{24} = 0, E_{25} = 0,\\
&E_{31} = 0, E_{32} = 0, E_{33} = \frac{\bar{e}_{31}^{(l,s)}k_x^2 + \bar{e}_{32}^{(l,s)}k_y^2 + 2\bar{e}_{36}^{(l,s)}k_xk_y}{\bar{\xi}_{11}^{(k,s)}k_x^2 + 2\bar{\xi}_{12}^{(k,s)}k_xk_y + \bar{\xi}_{22}^{(k,s)}k_y^2}, E_{34} = 0, E_{35} = 0,\\
&E_{41} = 0, E_{42} = 0, E_{43} = -\left(\mathrm{i}\omega C_R + \omega^2 C_L\right)\left(h_{c_2}\bar{e}_{31}^{(l,c)}k_x^2 + h_{c_2}\bar{e}_{32}^{(l,c)}k_y^2 + 2h_{c_2}\bar{e}_{36}^{(l,c)}k_xk_y\right),\\
&E_{44} = -\left(\mathrm{i}\omega C_R + \omega^2 C_L\right)\left(\bar{e}_{31}^{(l,c)}\mathrm{i}k_x + \bar{e}_{36}^{(l,c)}\mathrm{i}k_y\right),\\
&E_{45} = -\left(\mathrm{i}\omega C_R + \omega^2 C_L\right)\left(\bar{e}_{32}^{(l,c)}\mathrm{i}k_y + \bar{e}_{36}^{(l,c)}\mathrm{i}k_x\right).
\end{aligned}
\tag{57}
$$

2.1.5 Double piezoelectric layers with proportional derivative active control

LQR optimal control [19, 27], FXLMS adaptive algorithm [23] and PPF control [24, 44, 45] are employed in the modal space in order to suppress vibrations of the composite plates and shells with single-input single-output or multi-input multi-output configurations. It is complicated to perform single-input single-output feedback control in the wavenumber domain by using the Fourier and inverse Fourier transforms since point forces with feedback control can excite a great many coupled waves with different wavenumbers. The control strategies of LQR, FXLMS and PPF are not easy to apply. However, a proportional derivative control strategy for smart composite plates and shells with dense periodic feedback arrays [59] in the wavenumber domain can be used to avoid the difficulties in achieving the control methods of LQR, FXLMS and PPF. This is the reason why the proportional derivative control method is used in this work.

The output voltage of the sensor layer in the host plate is amplified by the external power circuits, which is fed back into the actuator layer to drive the constraining plate. Electric boundary conditions can be described by

$$
\Phi^{(l,c)}\big|_{Z=h_{c_1}} = 0,\ \Phi^{(l,c)}\big|_{Z=h_{c_2}} = V_e,\ D_3^{(l,s)}\Big|_{Z=h_{s_1}} = 0,\ \Phi^{(l,s)}\big|_{Z=h_{s_2}} = 0,
\tag{58}
$$

where V_e is the external control voltage. Proportional derivative control method is used to

control vibrations of the smart composite plate

$$V_e = -\left(G_p - \mathrm{i}\omega G_d\right)\Phi^{(l,s)}\big|_{Z=h_{s_1}}, \tag{59}$$

where G_p and G_d are the proportional and derivative gains, respectively. Substituting Eqs. (38) and (40) into Eq. (58) with the Fourier transform, one obtains

$$\begin{bmatrix} c_1 & c_2 & c_3 & c_4 \end{bmatrix}^{\mathrm{T}} = \left(\mathbf{G}^{(2)}\right)^{-1}\mathbf{E}^{(2)}\begin{bmatrix} \tilde{u}_1^{(s)} & \tilde{u}_2^{(s)} & \tilde{u}_3 & \tilde{u}_1^{(c)} & \tilde{u}_2^{(c)} \end{bmatrix}^{\mathrm{T}}, \tag{60}$$

where the elements $G_{ij}^{(2)}$ of the matrix $\mathbf{G}^{(2)}$ are given by

$$\begin{aligned}
&G_{11}^{(2)} = \mathrm{e}^{k_{p1}^{(c)}h_{c_1}}, G_{12}^{(2)} = \mathrm{e}^{k_{p2}^{(c)}h_{c_1}}, G_{13}^{(2)} = 0, G_{14}^{(2)} = 0,\\
&G_{21}^{(2)} = \mathrm{e}^{k_{p1}^{(c)}h_{c_2}}, G_{22}^{(2)} = \mathrm{e}^{k_{p2}^{(c)}h_{c_2}}, G_{23} = \left(G_p - \mathrm{i}\omega G_d\right)\mathrm{e}^{k_{p1}^{(s)}h_{s_1}}, G_{24} = \left(G_p - \mathrm{i}\omega G_d\right)\mathrm{e}^{k_{p2}^{(s)}h_{s_1}},\\
&G_{31}^{(2)} = 0, G_{32}^{(2)} = 0, G_{33}^{(2)} = \bar{\xi}_{33}^{(l,s)}k_{p1}^{(s)}\mathrm{e}^{k_{p1}^{(s)}h_{s_1}}, G_{34}^{(2)} = \bar{\xi}_{33}^{(l,s)}k_{p2}^{(s)}\mathrm{e}^{k_{p2}^{(s)}h_{s_1}},\\
&G_{41}^{(2)} = 0, G_{42}^{(2)} = 0, G_{43}^{(2)} = \mathrm{e}^{k_{p1}^{(s)}h_{s_2}}, G_{44}^{(2)} = \mathrm{e}^{k_{p2}^{(s)}h_{s_2}},
\end{aligned} \tag{61}$$

the elements $E_{ij}^{(2)}$ of the matrix $\mathbf{E}^{(2)}$ are defined by

$$\begin{aligned}
&E_{11}^{(2)} = 0, E_{12}^{(2)} = 0, E_{13}^{(2)} = \frac{\bar{e}_{31}^{(l,c)}k_x^2 + \bar{e}_{32}^{(l,c)}k_y^2 + 2\bar{e}_{36}^{(l,c)}k_xk_y}{\bar{\xi}_{11}^{(k,c)}k_x^2 + 2\bar{\xi}_{12}^{(l,c)}k_xk_y + \bar{\xi}_{22}^{(l,c)}k_y^2}, E_{14}^{(2)} = 0, E_{15}^{(2)} = 0,\\
&E_{21}^{(2)} = 0, E_{22}^{(2)} = 0, E_{23}^{(2)} = \frac{\bar{e}_{31}^{(l,c)}k_x^2 + \bar{e}_{32}^{(l,c)}k_y^2 + 2\bar{e}_{36}^{(l,c)}k_xk_y}{\bar{\xi}_{11}^{(l,c)}k_x^2 + 2\bar{\xi}_{12}^{(l,c)}k_xk_y + \bar{\xi}_{22}^{(l,c)}k_y^2}\\
&+\left(G_p - \mathrm{i}\omega G_d\right)\frac{\bar{e}_{31}^{(l,s)}k_x^2 + \bar{e}_{32}^{(l,s)}k_y^2 + 2\bar{e}_{36}^{(l,s)}k_xk_y}{\bar{\xi}_{11}^{(l,s)}k_x^2 + 2\bar{\xi}_{12}^{(l,s)}k_xk_y + \bar{\xi}_{22}^{(l,s)}k_y^2}, E_{24}^{(2)} = 0, E_{25}^{(2)} = 0,\\
&E_{31}^{(2)} = \bar{e}_{31}^{(l,s)}\mathrm{i}k_x + \bar{e}_{36}^{(l,s)}\mathrm{i}k_y, E_{32}^{(2)} = \bar{e}_{32}^{(l,s)}\mathrm{i}k_y + \bar{e}_{36}^{(l,s)}\mathrm{i}k_x,\\
&E_{33}^{(2)} = h_{s_1}\bar{e}_{31}^{(l,s)}k_x^2 + h_{s_1}\bar{e}_{32}^{(l,s)}k_y^2 + 2h_{s_1}\bar{e}_{36}^{(l,s)}k_xk_y, E_{34}^{(2)} = 0, E_{35}^{(2)} = 0,\\
&E_{41}^{(2)} = 0, E_{42}^{(2)} = 0, E_{43}^{(2)} = \frac{\bar{e}_{31}^{(l,s)}k_x^2 + \bar{e}_{32}^{(l,s)}k_y^2 + 2\bar{e}_{36}^{(l,s)}k_xk_y}{\bar{\xi}_{11}^{(l,s)}k_x^2 + 2\bar{\xi}_{12}^{(l,s)}k_xk_y + \bar{\xi}_{22}^{(l,s)}k_y^2}, E_{44}^{(2)} = 0, E_{45}^{(2)} = 0.
\end{aligned} \tag{62}$$

2.2 Solutions in the wavenumber domain

Substituting Eqs. (7), (8), (29), (30), (42)-(44) and (46)-(47) or (49)-(50), (55) or (60) into Eq. (19), performing Fourier transform and taking the variational operation, one obtains five governing equations for the constrained laminated plates with double piezoelectric layers. Solving the governing equations, one finds the natural frequencies and loss factors of the composite

plates with *small* damping using

$$\omega_R = \sqrt{\mathrm{Re}\left(\omega^2\right)} = 2\pi f,\ \eta = \mathrm{Im}\left(\omega^2\right)/\mathrm{Re}\left(\omega^2\right). \tag{63}$$

For the vibrations of composite plates with *large* damping, $\mathrm{Re}\left(\omega^2\right)$ in Eq. (63) can be negative. Therefore, the natural frequencies and loss factors of the composite plates should be defined by

$$\omega_R = \mathrm{Re}\left(\omega\right) = 2\pi f,\ \eta = \mathrm{Im}\left(\omega\right)/\mathrm{Re}\left(\omega\right). \tag{64}$$

The natural frequencies defined in Eqs. (63) and (64) are almost the same, but the loss factor in Eq. (63) is nearly twice as large as that in Eq. (64) with respect to the vibrations of composite plates with small damping. If a transverse unit point force f_p located at the point (x_0, y_0) acts on the composite plate, the Fourier transform of the external force is written as

$$\tilde{f}_p = \mathrm{e}^{-\mathrm{i}(k_x x_0 + k_y y_0)}. \tag{65}$$

Substituting Eq. (65) into the governing equations of the composite plates in the wavenumber domain, one obtains the transverse displacement spectra $\tilde{u}_3\left(k_x, k_y\right)$. The plane power spectral density (PPSD) of transverse displacements for the composite plates with respect to k_x and k_y is defined by

$$\mathrm{PPSD} = 20\log\left(\left|\tilde{u}_3\left(k_x, k_y\right)\right|/U_r\right), \tag{66}$$

where the reference wavenumber displacement U_r is given by $10^{-9}\mathrm{m}^3$

2.3 Cylindrical-wave spectral density of large circular composite plate in the cylindrical coordinate system

Taking the inverse Fourier transform of $\tilde{u}_3\left(k_x, k_y\right)$ with respect to k_x and k_y, one obtains the transverse displacement of the smart plates

$$u_3\left(x, y\right) = \frac{1}{4\pi^2}\int_{-\infty}^{+\infty}\int_{-\infty}^{+\infty}\tilde{u}_3\left(k_x, k_y\right)\mathrm{e}^{\mathrm{i}k_x x}\mathrm{e}^{\mathrm{i}k_y y}\mathrm{d}k_x\mathrm{d}k_y. \tag{67}$$

Transforming the rectangular coordinate system into the cylindrical coordinate system, one obtains

$$x = \alpha_3 \cos\alpha_2, y = \alpha_3 \sin\alpha_2, \tag{68}$$

where α_2 and α_3 are the circumferential angle and radial coordinate, respectively. k_x and k_y can be described by

$$k_x = k\cos\psi, k_y = k\sin\psi, \tag{69}$$

where k and ψ are the radial wavenumber and the propagation directivity angle of elastic waves. Substituting Eqs. (68) and (69) into Eq. (67), one obtains

$$u_3(\alpha_2, \alpha_3) = \frac{1}{4\pi^2}\int_0^{+\infty}\int_0^{2\pi} \tilde{u}_3(k\cos\psi, k\sin\psi)\, \mathrm{e}^{\mathrm{i}k\alpha_3\cos(\alpha_2-\psi)} k\mathrm{d}k\mathrm{d}\psi. \tag{70}$$

Expanding the exponential factor in Eq. (70), one obtains

$$\mathrm{e}^{\mathrm{i}k\alpha_3\cos(\alpha_2-\psi)} = \sum_{m=-\infty}^{+\infty} J_m(k\alpha_3)\, \mathrm{e}^{\mathrm{i}m(\alpha_2-\psi+\pi/2)} = \sum_{m=-\infty}^{+\infty} J_m(k\alpha_3)\, \mathrm{e}^{\mathrm{i}m\alpha_2}\mathrm{e}^{-\mathrm{i}m\psi}\mathrm{e}^{\mathrm{i}m\pi/2}, \tag{71}$$

where m is an integer and $J_m(k\alpha_3)$ is the Bessel function of the first kind with order m. In the far-field of transverse displacement for the smart plate, $J_m(k\alpha_3)$ can be expressed in asymptotic form for large k as

$$\begin{aligned} J_m(k\alpha_3) &= \frac{H_m^{(1)}(k\alpha_3) + H_m^{(2)}(k\alpha_3)}{2} \approx \left(\frac{2}{\pi k\alpha_3}\right)^{1/2} \cos\left(k\alpha_3 - \frac{\pi m}{2} - \frac{\pi}{4}\right) \\ &= \left(\frac{1}{2\pi k\alpha_3}\right)^{1/2} \mathrm{e}^{\mathrm{i}\left(k\alpha_3 - \frac{\pi m}{2} - \frac{\pi}{4}\right)} + \left(\frac{1}{2\pi k\alpha_3}\right)^{1/2} \mathrm{e}^{-\mathrm{i}\left(k\alpha_3 - \frac{\pi m}{2} - \frac{\pi}{4}\right)}. \end{aligned} \tag{72}$$

Substituting Eqs. (71) and (72) into Eq. (70), one obtains

$$\begin{aligned} u_3(\alpha_2, \alpha_3) \approx{}& \frac{1}{4\pi^2}\sum_{m=-\infty}^{+\infty}\int_0^{+\infty}\int_0^{2\pi} \tilde{u}_3(k\cos\psi, k\sin\psi)\, \mathrm{e}^{-\mathrm{i}m\psi} k^{1/2} \frac{\mathrm{e}^{\mathrm{i}\left(k\alpha_3 - \frac{\pi m}{2} - \frac{\pi}{4}\right)}}{\sqrt{2\pi\alpha_3}} \mathrm{d}k\mathrm{d}\psi \mathrm{e}^{\mathrm{i}m\pi/2}\mathrm{e}^{\mathrm{i}m\alpha_2} \\ &+ \frac{1}{4\pi^2}\sum_{m=-\infty}^{+\infty}\int_0^{+\infty}\int_0^{2\pi} \tilde{u}_3(k\cos\psi, k\sin\psi)\, \mathrm{e}^{-\mathrm{i}m\psi} k^{1/2} \frac{\mathrm{e}^{-\mathrm{i}\left(k\alpha_3 - \frac{\pi m}{2} - \frac{\pi}{4}\right)}}{\sqrt{2\pi\alpha_3}} \mathrm{d}k\mathrm{d}\psi \mathrm{e}^{\mathrm{i}m\pi/2}\mathrm{e}^{\mathrm{i}m\alpha_2}. \end{aligned} \tag{73}$$

The first and second terms on the right-hand side of Eq. (73) represent the outgoing elastic waves and inwardly going waves, respectively. Cylindrical-wave spectral density (CSD) of the

transverse displacement for the composite plates in the far field is defined by

$$\mathrm{CSD} = \left| \frac{1}{(2\pi)^{5/2}} \int_0^{2\pi} \tilde{u}_3 \left(k\cos\psi, k\sin\psi\right) \mathrm{e}^{-\mathrm{i}m\psi} k^{1/2} \mathrm{d}\psi \right|. \tag{74}$$

Energy of the transverse displacement for the composite plate is given by [61]

$$\int_{-\infty}^{\infty}\int_{-\infty}^{\infty} u_3 u_3^* \mathrm{d}x\mathrm{d}y = \frac{1}{4\pi^2}\int_{-\infty}^{\infty}\int_{-\infty}^{\infty} \tilde{u}_3 \tilde{u}_3^* \mathrm{d}k_x \mathrm{d}k_y, \tag{75}$$

where the star symbol denotes the complex conjugate. Substituting Eq. (69) into Eq. (75), one obtains

$$\int_{-\infty}^{\infty}\int_{-\infty}^{\infty} u_3 u_3^* \mathrm{d}x\mathrm{d}y = \frac{1}{4\pi^2}\int_0^{+\infty}\int_0^{2\pi} \tilde{u}_3 \left(k\cos\psi, k\sin\psi\right) \tilde{u}_3^* \left(k\cos\psi, k\sin\psi\right) k\mathrm{d}k\mathrm{d}\psi. \tag{76}$$

The radial power spectral density (RPSD) of the transverse displacement for the composite plate with regards to (k, ψ) is defined by

$$\mathrm{RPSD} = \frac{\left|\tilde{u}_3 \left(k\cos\psi, k\sin\psi\right)\right| k^{1/2}}{2\pi}. \tag{77}$$

CSD in Eq. (74) can be used to distinguish which kinds of the cylindrical waves with special circumferential wavenumber dominate transverse vibration of the composite plates. RPSD in Eq. (77) can be employed to identify the propagation directions and energy of the elastic waves.

3 Numerical results

The material parameters of the sandwich plates considered in the following are listed in Table 1, where h is the thickness of the lamina. The piezoelectric layer is made of PZT material. Piezoelectric and dielectric constants e_{31}, e_{32}, ξ_{11}, ξ_{22} and ξ_{33} of the smart layer are $-6.5\mathrm{C/m}^2$, $-6.5\mathrm{C/m}^2$, $1.503\times10^{-8}\mathrm{F/m}$, $1.503\times10^{-8}\mathrm{F/m}$, $1.3\times10^{-8}\mathrm{F/m}$, respectively. Free vibrations of the constrained composite damping plate with a single piezoelectric layer investigated by Gao and Shen [4] are used here to compare with the present results. The constrained piezoelectric composite plate [4] is composed of two face plates with a damping core described in Table 1. The constraining plate is the PZT piezoelectric layer, the material of the host plate is listed as "lamina 1" in Table 1. The length a and width b of the rectangular sandwich plate in the x and y directions are 0.3m and 0.4m, respectively. k_x and k_y of the simply supported

Table 1: Material parameters of the sandwich plates

Material	E_1 (GPa)	E_2 (GPa)	ν_{12}	$\rho\left(\mathrm{kg/m^3}\right)$	h (mm)	α (Rad)
PZT	49	49	0.3	7500	1	0
Lamina 1	70	70	0.33	1104	3	0
Damping core	$2.5088\,(1-0.5\mathrm{i})\times 10^{-3}$	$2.5088\,(1-0.5\mathrm{i})\times 10^{-3}$	0.4	999	2	0
Boron-epoxy	207	20.7	0.3	2000	3	0

Table 2: Natural frequencies and loss factors of the constrained composite damping plate without piezoelectric effects

(m,n)	f (Hz) [4]	η [4]	f (Hz) present solution	η present solution
$(1,1)$	113.3	8.41×10^{-2}	113.3	8.41×10^{-2}
$(1,2)$	224.6	4.72×10^{-2}	224.6	4.73×10^{-2}
$(1,3)$	409.4	2.73×10^{-2}	409.5	2.72×10^{-2}
$(2,1)$	310.9	3.52×10^{-2}	310.9	3.52×10^{-2}
$(2,2)$	421.8	2.65×10^{-2}	421.8	2.65×10^{-2}
$(2,3)$	606.4	1.88×10^{-2}	606.6	1.88×10^{-2}
$(3,3)$	934.7	1.23×10^{-2}	934.9	1.23×10^{-2}

composite plate are $m\pi/a$ and $n\pi/b$, respectively. Natural frequencies and loss factors of the piezoelectric sandwich plates are calculated using Eq. (63).

The natural frequencies and loss factors of the constrained sandwich plate without piezoelectric effects are listed in Table 2. The natural frequencies and loss factors of the composite plate with piezoelectric effects under the open circuit boundary conditions are given in Table 3. The present results are in good agreement with those from Gao and Shen's work [4] also in Tables 2 and 3. We conclude that the formulae used in this work are feasible and valid. Piezoelectric effects of the single piezoelectric layer do not make a significant impact on the natural frequencies and loss factors of the constrained composite plate with open circuit boundary conditions.

Table 3: Natural frequencies and loss factors of the constrained composite damping plate with a single piezoelectric layer

(m,n)	f (Hz) open circuit [4]	η open circuit [4]	f (Hz) open circuit, present solution	η open circuit, present solution
$(1,1)$	113.4	8.44×10^{-2}	113.4	8.44×10^{-2}
$(1,2)$	224.8	4.73×10^{-2}	224.8	4.73×10^{-2}
$(1,3)$	409.7	2.73×10^{-2}	409.8	2.72×10^{-2}
$(2,1)$	311.1	3.52×10^{-2}	311.2	3.52×10^{-2}
$(2,2)$	422.1	2.65×10^{-2}	422.1	2.65×10^{-2}
$(2,3)$	606.9	1.87×10^{-2}	607.0	1.87×10^{-2}
$(3,3)$	934.4	1.23×10^{-2}	935.6	1.23×10^{-2}

3.1 Free vibrations of the constrained piezoelectric composite plate with closed or open circuit boundary conditions

The constrained composite damping plate in Table 3 is still employed in the following discussion but the bottom surface of the isotropic host plate is attached to the piezoelectric layer listed in Table 1. The natural frequencies and loss factors of the constrained composite damping plate with double piezoelectric layers are depicted in Table 4. Electric boundary conditions of the two smart layers are closed or open circuits. The natural frequencies and loss factors of the composite plate without piezoelectric effects (called by 'bare plate') are also shown in Table 4. The natural frequencies of the composite plate with open circuit boundary conditions have the largest frequency values in compared to the other cases. Piezoelectric effects of double piezoelectric layers play a minor role in free vibration of the passive constrained composite plate. The reason why the natural frequencies are shifted up from those of the bare plate for the open circuit condition and back down for the closed circuit condition in Table 4 is due to different contributions of the electric potentials in the piezoelectric layers with open or closed circuits to the governing equations of the smart composite plate. Using the material parameters of the piezoelectric layers and simplifying Eq. (46), one obtains

$$\begin{bmatrix} c_1 \\ c_2 \end{bmatrix} = \begin{bmatrix} \mathrm{e}^{k_{p1}^{(c)} h_{c_1}} & \mathrm{e}^{k_{p2}^{(c)} h_{c_1}} \\ \mathrm{e}^{k_{p1}^{(c)} h_{c_2}} & \mathrm{e}^{k_{p2}^{(c)} h_{c_2}} \end{bmatrix}^{-1} \begin{bmatrix} 1 \\ 1 \end{bmatrix} \frac{\bar{e}_{31}^{(k,c)}}{\bar{\xi}_{11}^{(k,c)}} \tilde{u}_3. \tag{78}$$

Similarly, simplifying Eq. (49), one obtains

$$\begin{aligned} \begin{bmatrix} c_1 \\ c_2 \end{bmatrix} &= \frac{1}{\bar{\xi}_{33}^{(k,c)} k_{p1}^{(c)}} \begin{bmatrix} \mathrm{e}^{k_{p1}^{(c)} h_{c_1}} & -\mathrm{e}^{k_{p2}^{(c)} h_{c_1}} \\ \mathrm{e}^{k_{p1}^{(c)} h_{c_2}} & -\mathrm{e}^{k_{p2}^{(c)} h_{c_2}} \end{bmatrix}^{-1} \begin{bmatrix} \bar{e}_{31}^{(k,c)} \mathrm{i} k_x & \bar{e}_{32}^{(k,c)} \mathrm{i} k_y & h_{c_1} \bar{e}_{31}^{(k,c)} k_x^2 + h_{c_1} \bar{e}_{32}^{(k,c)} k_y^2 \\ \bar{e}_{31}^{(k,c)} \mathrm{i} k_x & \bar{e}_{32}^{(k,c)} \mathrm{i} k_y & h_{c_2} \bar{e}_{31}^{(k,c)} k_x^2 + h_{c_2} \bar{e}_{32}^{(k,c)} k_y^2 \end{bmatrix} \begin{bmatrix} \tilde{u}_1^{(c)} \\ \tilde{u}_2^{(c)} \\ \tilde{u}_3 \end{bmatrix} \\ &= \begin{bmatrix} \mathrm{e}^{k_{p1}^{(c)} h_{c_1}} & -\mathrm{e}^{k_{p2}^{(c)} h_{c_1}} \\ \mathrm{e}^{k_{p1}^{(c)} h_{c_2}} & -\mathrm{e}^{k_{p2}^{(c)} h_{c_2}} \end{bmatrix}^{-1} \begin{bmatrix} \frac{\mathrm{i} k_x}{k_{p1}^{(c)}} & \frac{\mathrm{i} k_y}{k_{p1}^{(c)}} & \frac{h_{c_1}\left(k_x^2+k_y^2\right)}{k_{p1}^{(c)}} \\ \frac{\mathrm{i} k_x}{k_{p1}^{(c)}} & \frac{\mathrm{i} k_y}{k_{p1}^{(c)}} & \frac{h_{c_2}\left(k_x^2+k_y^2\right)}{k_{p1}^{(c)}} \end{bmatrix} \begin{bmatrix} \tilde{u}_1^{(c)} \\ \tilde{u}_2^{(c)} \\ \tilde{u}_3 \end{bmatrix} \frac{\bar{e}_{31}^{(k,c)}}{\bar{\xi}_{33}^{(k,c)}}. \end{aligned} \tag{79}$$

By using the parameters in Tables 1 and 4, the elements in Eq. (79) have the following relation

$$\frac{h_{c_1}\left(k_x^2+k_y^2\right)}{k_{p1}^{(c)}} \ll \frac{k_x}{k_{p1}^{(c)}}, \frac{h_{c_1}\left(k_x^2+k_y^2\right)}{k_{p1}^{(c)}} \ll \frac{k_y}{k_{p1}^{(c)}}, \frac{h_{c_1}\left(k_x^2+k_y^2\right)}{k_{p1}^{(c)}} \ll 1. \tag{80}$$

Table 4: Natural frequencies and loss factors of the constrained composite damping plate with double piezoelectric layers

(m,n)	f (Hz) open circuit	η open circuit	f (Hz) closed circuit	η closed circuit	f (Hz) bare plate	η bare plate
$(1,1)$	123.7	5.40×10^{-2}	122.4	5.45×10^{-2}	122.3	5.45×10^{-2}
$(1,2)$	249.8	2.92×10^{-2}	247.0	2.95×10^{-2}	246.8	2.95×10^{-2}
$(1,3)$	459.4	1.64×10^{-2}	454.3	1.67×10^{-2}	453.9	1.67×10^{-2}
$(2,1)$	347.6	2.14×10^{-2}	343.7	2.17×10^{-2}	343.4	2.17×10^{-2}
$(2,2)$	473.4	1.60×10^{-2}	468.1	1.62×10^{-2}	467.7	1.62×10^{-2}
$(2,3)$	683.0	1.12×10^{-2}	675.2	1.14×10^{-2}	674.7	1.14×10^{-2}
$(3,1)$	720.2	1.06×10^{-2}	712.1	1.08×10^{-2}	711.5	1.08×10^{-2}
$(3,2)$	846.0	0.91×10^{-2}	836.3	0.93×10^{-2}	835.7	0.92×10^{-2}
$(3,3)$	1055.5	0.73×10^{-2}	1043.5	0.74×10^{-2}	1042.7	0.74×10^{-2}

Therefore, $\tilde{u}_1^{(c)}$ and $\tilde{u}_2^{(c)}$ play an important role in c_1 and c_2 of Eq. (79). It is shown that contributions of $\tilde{u}_3$ to c_1 and c_2 in Eq. (78) are much larger than that of $\tilde{u}_3$ to c_1 and c_2 in Eq. (79). According to Eqs. (42)-(44), Eqs. (29)-(30), Eqs. (78)-(79) and the simplified formulae of Eqs. (47) and (50), it is found that the electric potentials of the piezoelectric layers affect the governing equations of the smart sandwich plate by the transverse displacement spectra $\tilde{u}_3$ with respect to closed circuit boundary conditions. Those affect the equations of motion of the smart sandwich plates by the in-plane displacement spectra $\tilde{u}_1^{(c)}$, $\tilde{u}_2^{(c)}$, $\tilde{u}_1^{(s)}$ and $\tilde{u}_2^{(s)}$ in the case of the open circuit boundary conditions. These two coupling effects of the piezoelectric layers will produce different bending stiffnesses and cause increase of the natural frequencies in comparison with those of the bare plate. The piezoelectric layers with open circuit boundary conditions give rise to larger natural frequencies than those with closed circuit boundary conditions since bending stiffnesses of the smart sandwich plate with open circuit boundary conditions are larger than those with closed circuit boundary conditions.

3.2 Free vibrations of a constrained composite damping plate with sensor and actuator layers under feedback control

The natural frequencies and loss factors of a constrained composite plate with sensor and actuator layers connected by an external dielectric slab with uniform resistances and inductances are presented in Table 5. Natural frequencies of the constrained composite damping plate have small differences in comparison with those shown in Table 4 when the external resistances and inductances are connected to the two piezoelectric layers. The loss factors are also only slightly changed, as shown by the results presented in Tables 4 and 5. The dielectric slab with

Table 5: The natural frequencies and loss factors of the constrained composite damping plate with sensor and actuator layers connected by an external dielectric slab with uniform resistances and inductances

(m,n)	f (Hz) $C_R = 100,\ C_L = 0$	η $C_R = 100,\ C_L = 0$	f (Hz) $C_R = 0,\ C_L = 1$	η $C_R = 0,\ C_L = 1$
$(1,1)$	123.4	5.11×10^{-2}	124.1	5.45×10^{-2}
$(1,2)$	249.2	2.42×10^{-2}	250.0	2.97×10^{-2}
$(1,3)$	459.0	1.20×10^{-2}	459.7	1.68×10^{-2}
$(2,1)$	347.1	1.65×10^{-2}	347.8	2.19×10^{-2}
$(2,2)$	473.0	1.16×10^{-2}	473.6	1.63×10^{-2}
$(2,3)$	682.7	0.77×10^{-2}	683.2	1.14×10^{-2}
$(3,1)$	720.0	0.73×10^{-2}	720.4	1.09×10^{-2}
$(3,2)$	845.8	0.62×10^{-2}	846.2	0.93×10^{-2}
$(3,3)$	1055.4	0.49×10^{-2}	1055.7	0.75×10^{-2}

uniform resistances and inductances doesn't remarkably affect the free vibrational features of the smart composite plates. The natural frequencies and loss factors of the piezoelectric constrained sandwich plate with $C_R \in [0, 100]$ and $C_L \in [0, 1]$ are close to those in the case of $(C_R = 100, C_L = 0)$ and $(C_R = 0, C_L = 1)$. The results from $C_R \in [0, 100]$ and $C_L \in [0, 1]$ are not markedly different in comparison with those shown in Table 5. Therefore, the natural frequencies and loss factors of the constrained composite damping plate with resistance and inductance parameters $C_R \in [0, 100]$, $C_L \in [0, 1]$ are not listed in Table 5. The electrical energy stored in the double piezoelectric layers is much smaller than the mechanical energy of the composite plate.

The natural frequencies and loss factors of the constrained composite damping plate with sensor and actuator layers are listed in Table 6 when proportional derivative active control is employed. The loss factors of the smart plate with $G_p = 0$ and $G_d = 0.2$ are much larger than those given in Tables 4 and 5. G_d has thus significant influence on the damping characteristics of the composite plate. The natural frequencies of the composite plate with $G_p = 200$ and $G_d = 0$ are smaller than those shown in Tables 4 and 5. G_p primarily affects the natural frequencies of a smart composite plate and leads to a moderate increase of the damping factors. In Table 6, the natural frequencies of the composite plate with $G_p = 200$ and $G_d = 0$ are almost between those of the composite plate with $\left(G_p = 0, G_d = 0.2\right)$ and those with $\left(G_p = 200, G_d = 0.2\right)$, and the damping factors further rise for $\left(G_p = 200, G_d = 0.2\right)$. Active control of the constrained damping layer changes the free vibration features of the composite plate and has better performance on vibration suppression than that based on passive control.

The effects of G_d on the natural frequencies and loss factors of the propagating waves

Table 6: The natural frequencies and loss factors of the constrained composite damping plate with sensor and actuator layers under active control

(m,n)	f (Hz) $G_p=0$, $G_d=0.2$	η $G_p=0$, $G_d=0.2$	f (Hz) $G_p=200$, $G_d=0$	η $G_p=200$, $G_d=0$	f (Hz) $G_p=200$, $G_d=0.2$	η $G_p=200$, $G_d=0.2$
$(1,1)$	128.6	4.01×10^{-1}	89.2	2.91×10^{-1}	87.2	9.08×10^{-1}
$(1,2)$	259.2	4.52×10^{-1}	215.0	1.22×10^{-1}	217.2	6.59×10^{-1}
$(1,3)$	476.2	4.77×10^{-1}	424.5	6.27×10^{-2}	433.8	5.83×10^{-1}
$(2,1)$	360.5	4.67×10^{-1}	312.8	8.45×10^{-2}	318.2	6.10×10^{-1}
$(2,2)$	490.6	4.78×10^{-1}	438.5	6.07×10^{-2}	448.2	5.81×10^{-1}
$(2,3)$	707.3	4.88×10^{-1}	648.0	4.14×10^{-2}	664.8	5.58×10^{-1}
$(3,1)$	745.8	4.89×10^{-1}	685.2	3.91×10^{-2}	703.3	5.55×10^{-1}
$(3,2)$	875.6	4.93×10^{-1}	810.9	3.32×10^{-2}	833.1	5.48×10^{-1}
$(3,3)$	1091.8	4.97×10^{-1}	1020.4	2.64×10^{-2}	1049.3	5.41×10^{-1}

defined by $(m=1,n=1)$ and $(m=1,n=2)$ are shown in Fig. 4 for $G_p=0$. Note that natural frequencies and loss factors are calculated using Eq. (64) since the loss factors can be larger than 1. Natural frequencies of the propagating waves increase in the beginning and afterwards decrease as G_d rises. However, loss factors are slightly reduced in the beginning and subsequently increase. Damping of the composite plate increases distinctly when G_d is larger than 0.1. The natural frequencies have larger values when G_d is between 0.2 and 0.3. The influence of G_p on the natural frequencies and loss factors of the propagating waves is shown in Fig. 5 for $G_d=0.2$. The natural frequencies decrease and the loss factors increase as G_p grows. The bending stiffnesses of the piezoelectric constraining layer reduce as G_p increases. G_p results in a moderate rise of the damping factors. In Table 6 and Fig. 4, an appropriate derivative gain G_d can attenuate vibrations of the composite plates to a great extent. The derivative gain G_d has good performance on vibration suppression of the composite plates and shells with piezoelectric layers [6, 29, 60, 72–75]. The piezoelectric sandwich damping plate has excellent damping features when G_d increases from 0.6 to 1.0 in Fig. 4(b). Active control of the smart composite plates with large derivative gains can thus easily give rise to large damping. Li and Yang [72] explored active control of vibrations for piezoelectric laminated cylindrical shells with sensor and actuator layers in detail using the state space method and showed the excellent features of vibration reduction via the derivative feedback control. Derivative gain G_d is more favourable to suppress vibrations of the smart sandwich plates than proportional gain G_p by comparing Fig. 4(b) with Fig. 5(b). The damping effects of the piezoelectric sandwich damping plates with proportional derivative control strategy on suppression of transverse vibrations are better than those of the passive sandwich damping plates.

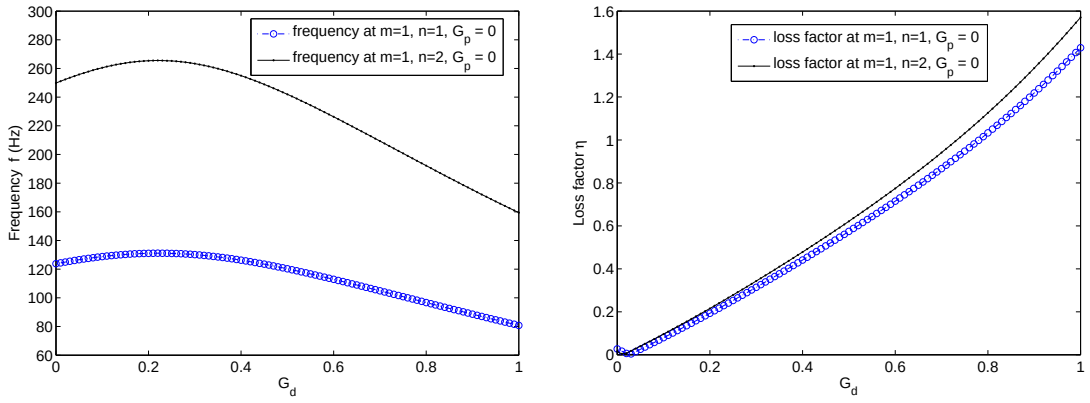

(a) (b)

Figure 4: (a) Effects of G_d on the natural frequencies of the propagating waves $(m = 1, n = 1)$ and $(m = 1, n = 2)$; (b) Effects of G_d on the loss factors of the propagating waves $(m = 1, n = 1)$ and $(m = 1, n = 2)$

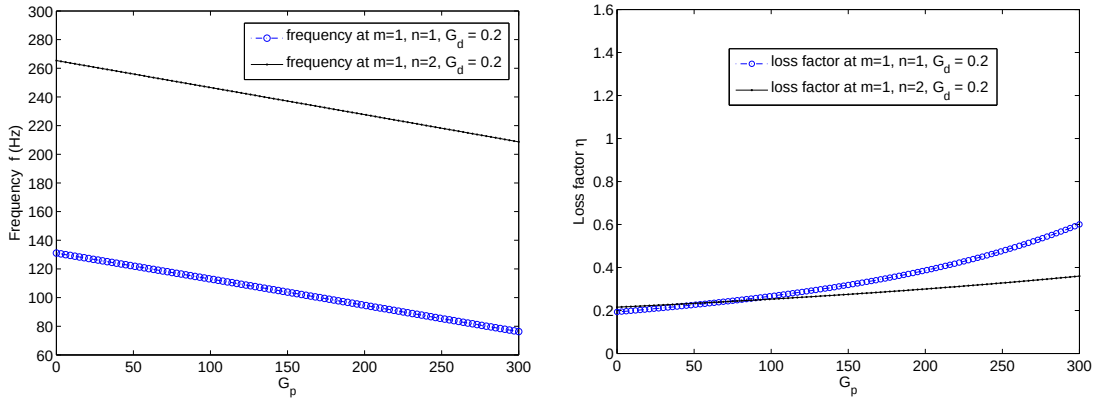

(a) (b)

Figure 5: (a) Effects of G_p on the natural frequencies of the propagating waves $(m = 1, n = 1)$ and $(m = 1, n = 2)$; (b) Effects of G_p on the loss factors of the propagating waves $(m = 1, n = 1)$ and $(m = 1, n = 2)$

3.3 Forced vibrations of the constrained composite damping plate with double piezoelectric layers under active control

PPSD of the transverse displacement for the constrained composite damping plate with double piezoelectric layers driven by a unit point force located at the origin is shown in Fig. 6 at 1kHz. The average transverse displacement of the constrained composite plate with $\left(G_p = 0, G_d = 0\right)$ is the largest compared with other PPSDs shown in Figs. 6(b)-6(d). The transverse vibrations of the composite plate with $\left(G_p = 0, G_d = 0.2\right)$ and $\left(G_p = 200, G_d = 0.2\right)$ are notably suppressed. The average transverse displacement of the composite plate with $G_p = 200$ and $G_d = 0.2$ has the smallest value of those shown in Fig. 6. CSD of the far-field transverse displacement for the constrained laminated damping plate with double piezoelectric layers under active control at 1kHz has only one strip pattern and the only circumferential wavenumber m is 0. Elastic waves of the transverse displacement in the constrained laminated damping plate with two piezoelectric layers are independent of the circumferential wavenumber since the exciting point force is located at the origin of the local coordinate system for the host plate. $\tilde{u}_3$ of the smart composite plate with transversely isotropic materials is only associated with the radial wavenumber k. The dominant spectral distribution is between radial wavenumbers $k = 35$ and $k = 40$ in Fig. 6(d).

The governing equations for smart laminated plates can be described by a complex matrix with five rows and columns, and one loading vector. Therefore, a reduced equation of the smart plate driven by a unit point force can be obtained for the transverse displacement spectra $\tilde{u}_3$,

$$\tilde{u}_3 = \mathrm{e}^{-\mathrm{i}\left(k_x x_0 + k_y y_0\right)} / D_w\left(k\right), k = \left(k_x^2 + k_y^2\right)^{1/2}, \tag{81}$$

where $D_w\left(k\right)$ is the spectral stiffness with respect to the transverse displacement and extracted from the governing equations for the smart laminated plate. The factor $\mathrm{e}^{-\mathrm{i}\left(k_x x_0 + k_y y_0\right)}$ in Eq. (81) can be expressed by

$$\begin{aligned} &\mathrm{e}^{-\mathrm{i}\left(k_x x_0 + k_y y_0\right)} = \mathrm{e}^{-\mathrm{i}k\bar{\alpha}_3 \cos(\bar{\alpha}_2 - \psi)} = \sum_{m_1=-\infty}^{+\infty} J_{m_1}\left(k\bar{\alpha}_3\right) \mathrm{e}^{-\mathrm{i}m_1\bar{\alpha}_2} \mathrm{e}^{\mathrm{i}m_1\psi} \mathrm{e}^{-\mathrm{i}m_1\pi/2}, \\ &\bar{\alpha}_3 = \left(x_0^2 + y_0^2\right)^{1/2}, \bar{\alpha}_2 = \mathrm{atan}\left(y_0/x_0\right) \text{ or } \mathrm{atan}\left(y_0/x_0\right) + \pi, \end{aligned} \tag{82}$$

where m_1 is an integer. Substituting Eqs. (81) and (82) into Eq. (74) in the case of $\bar{\alpha}_3 = 0$, one

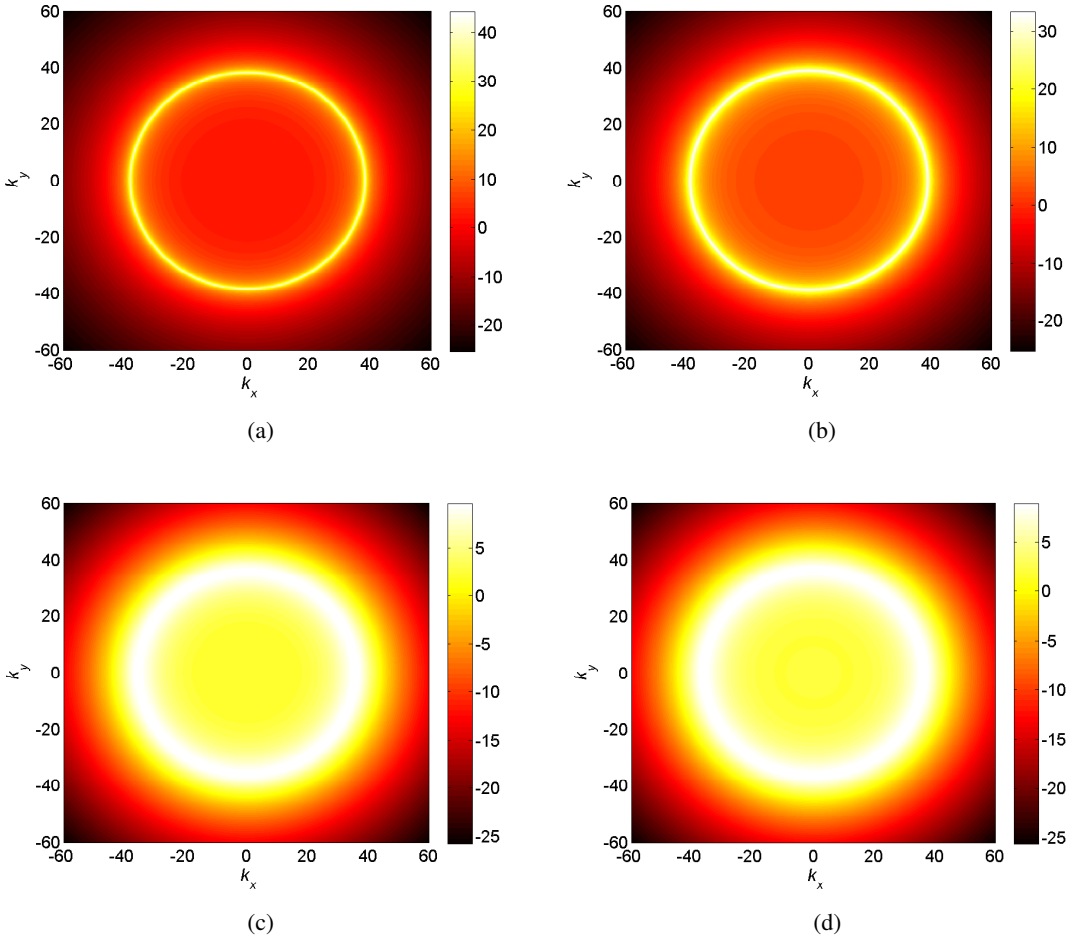

Figure 6: (a) PPSD of transverse displacement for the constrained composite damping plate with double piezoelectric layers at 1kHz, $\left(G_p = 0, G_d = 0\right)$; (b) PPSD of transverse displacement for the constrained composite damping plate with double piezoelectric layers at 1kHz, $\left(G_p = 200, G_d = 0\right)$; (c) PPSD of transverse displacement for the constrained composite damping plate with double piezoelectric layers at 1kHz, $\left(G_p = 0, G_d = 0.2\right)$; (d) PPSD of transverse displacement for the constrained composite damping plate with double piezoelectric layers at 1kHz, $\left(G_p = 200, G_d = 0.2\right)$

obtains

$$\mathrm{CSD} = \begin{cases} \left|\frac{J_0(k\bar{\alpha}_3)k^{1/2}}{(2\pi)^{3/2}D_w(k)}\right|, (\bar{\alpha}_3 = 0, m = 0), \\ 0, (\bar{\alpha}_3 = 0, m \neq 0). \end{cases} \tag{83}$$

When the point force is not at the origin, one obtains

$$\mathrm{CSD} = \left|\frac{J_m(k\bar{\alpha}_3)\,k^{1/2}}{(2\pi)^{3/2}D_w(k)}\right|. \tag{84}$$

A great many cylindrical waves of the transverse displacement with different circumferential wavenumber propagate in the composite plate.

The first lamina of the host face plate shown in Fig. 1 is replaced with an orthotropic boron-epoxy material in order to study vibrations of the composite plates with nonuniform in-plane stiffnesses in the following discussion. The material parameters of the orthotropic lamina are listed in Table 1. The other layers of the composite plates with double piezoelectric laminas are kept unchanged. The constrained composite damping plate with two piezoelectric layers is then not transversely isotropic any more. CSD of the far-field transverse displacement for the constrained composite damping plate with two piezoelectric layers under $\left(G_p = 200, G_d = 0.2\right)$ is shown in Fig. 7 at 1kHz and 1.5kHz. Some elastic waves with special circumferential wavenumbers propagate in the composite plate due to the orthotropic layer of the host plate. The spectral stiffness D_w of the sandwich plate is associated with k and ψ, and the influence of the orthotropic layer on the far-field transverse displacement is important in Fig. 7. Only the waves with even circumferential wavenumber exist in the composite plate when the transverse point force drives it at the origin. The patterns of far-field CSD slowly change with circumferential wavenumber as a result of large active constrained damping when the circular frequency increases. However, the main radial wavenumber has a moderate shift in Fig. 7(b). The reduced equation of the transverse displacement spectra for the smart sandwich plate is described as

$$\tilde{u}_3 = \mathrm{e}^{-\mathrm{i}\left(k_x x_0 + k_y y_0\right)}/D_w(k,\psi). \tag{85}$$

Substituting Eqs. (85) and (82) into Eq. (74), one obtains

$$\mathrm{CSD} = \left|\frac{1}{(2\pi)^{5/2}}\int_0^{2\pi}\sum_{m_1=-\infty}^{+\infty}\left(J_{m_1}(k\bar{\alpha}_3)\,\mathrm{e}^{-\mathrm{i}m_1\bar{\alpha}_2}\mathrm{e}^{\mathrm{i}m_1\psi}\mathrm{e}^{-\mathrm{i}m_1\pi/2}/D_w(k,\psi)\right)\mathrm{e}^{-\mathrm{i}m\psi}k^{1/2}\mathrm{d}\psi\right|. \tag{86}$$

With a point force located at $(0,0)$, Eq. (86) can be further simplified to obtain

$$\mathrm{CSD} = \left| \frac{1}{(2\pi)^{5/2}} \left(\int_0^{\pi} \frac{\mathrm{e}^{-\mathrm{i}m\psi}}{D_w(k,\psi)} k^{1/2} \mathrm{d}\psi + \int_0^{\pi} \frac{(-1)^m \mathrm{e}^{-\mathrm{i}m\psi}}{D_w(k,\psi+\pi)} k^{1/2} \mathrm{d}\psi \right) \right|. \tag{87}$$

For the present composite plate

$$D_w(k,\psi) = D_w(k,\psi+\pi) \tag{88}$$

holds. This equation can be verified by a numerical test. Substituting Eq. (88) into Eq. (87), one obtains

$$\mathrm{CSD} = \begin{cases} \left| \frac{2}{(2\pi)^{5/2}} \int_0^{\pi} \frac{\mathrm{e}^{-\mathrm{i}m\psi}}{D_w(k,\psi)} k^{1/2} \mathrm{d}\psi \right|, m = 2m_1, \\ 0, m = 2m_1 + 1. \end{cases} \tag{89}$$

This is the reason why the alternating stripe pattern appears in Fig. 7. CSD of the far-field transverse displacement has a complicated patterns when the driving force is not located at the origin. Magliula et al. [76] analytically presented a formula for the far-field transverse displacement of an anisotropic plate in the wavenumber domain using the stationary phase method. It is easy to prove that the far-field CSD of the anisotropic plate is zero for odd circumferential wavenumbers with a point force located at the origin.

RPSD of the transverse displacement for the constrained composite damping plate with double piezoelectric layers under $\left(G_p = 200, G_d = 0.2\right)$ is shown in Fig. 8 at 1kHz and 1.5kHz. The vertical coordinate in Fig. 8 denotes the propagation directivity angle (circumferential angle) of the elastic wave. The orthotropic layer of the host plate has a significant effect on RPSD and predominant elastic waves propagate in the directions approaching 0 and π. The spectral patterns in Fig. 8(b) are similar to those in Fig. 8(a). The phase angles of the transverse displacement spectra $\tilde{u}_3$ for the constrained composite damping plate with two piezoelectric layers driven by a point force are shown in Fig. 9 at 1kHz and 1.5kHz under $\left(G_p = 200, G_d = 0.2\right)$. In Fig. 9, the phase angles belong to $[-\pi/2, 3\pi/2]$. Some phase angles approaching 2 do not exist. Phase angles of the elastic waves with the same propagation directivity angle smoothly vary due to the large damping. The phase angles of the elastic waves can be influenced by the location of the force. Eq. (77) can be used to show that RPSD is independent of the point force location.

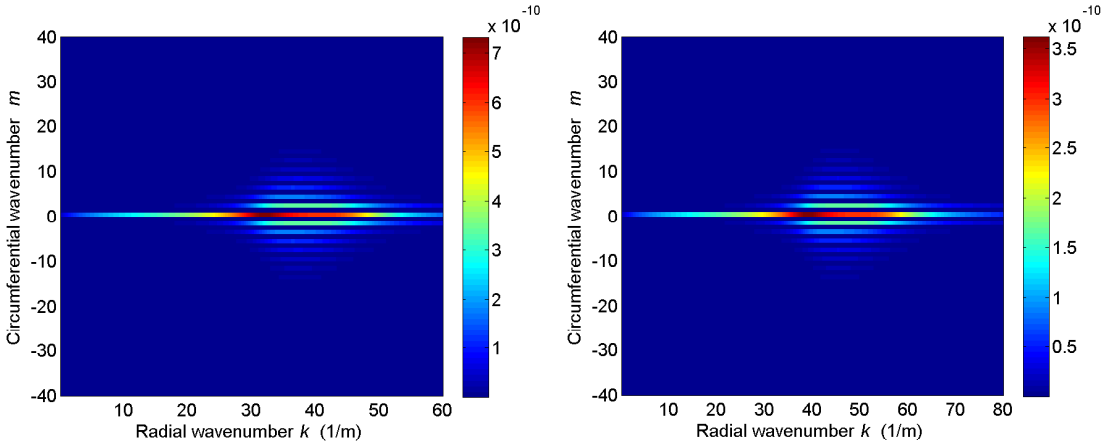

(a) (b)

Figure 7: (a) CSD of the far-field transverse displacement for the constrained composite damping plate with double piezoelectric layers at 1kHz, $\left(G_p = 200, G_d = 0.2\right)$, $(x_0 = 0, y_0 = 0)$; (b) CSD of the far-field transverse displacement for the constrained composite damping plate with double piezoelectric layers at 1.5kHz, $\left(G_p = 200, G_d = 0.2\right)$, $(x_0 = 0, y_0 = 0)$

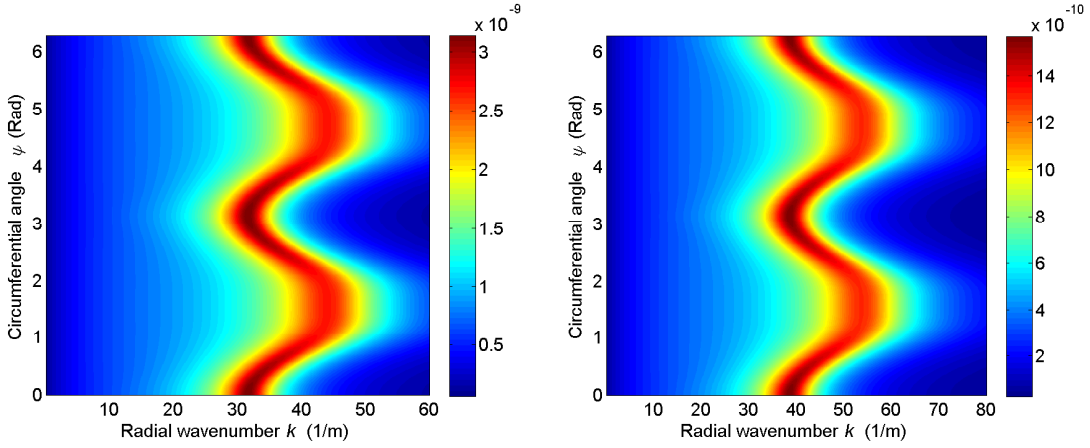

(a) (b)

Figure 8: (a) RPSD of the constrained composite damping plate with double piezoelectric layers at 1kHz, $\left(G_p = 200, G_d = 0.2\right)$, $(x_0 = 0, y_0 = 0)$; (b) RPSD of the constrained composite damping plate with double piezoelectric layers at 1.5kHz, $\left(G_p = 200, G_d = 0.2\right)$, $(x_0 = 0, y_0 = 0)$

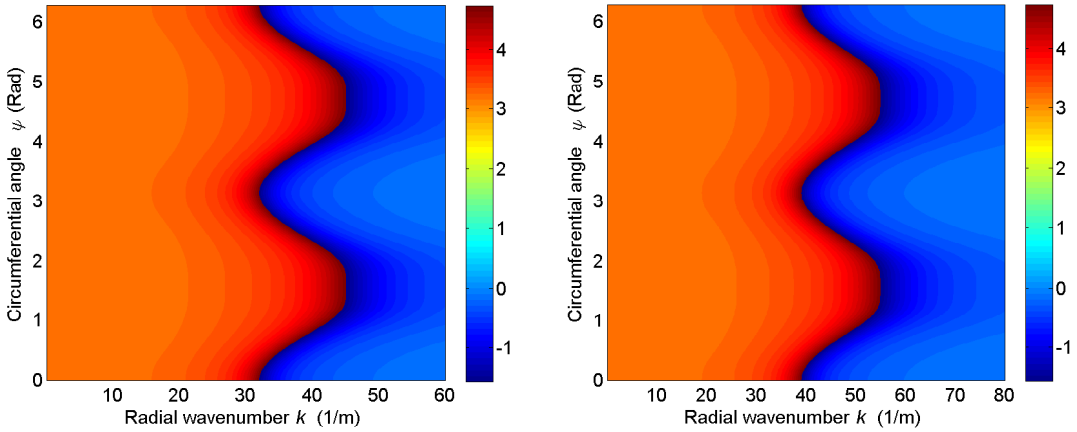

(a) (b)

Figure 9: (a) Phase angles of the transverse displacement spectra for the constrained composite damping plate with two piezoelectric layers driven by a point force at 1kHz, $\left(G_p = 200, G_d = 0.2\right)$, $(x_0 = 0, y_0 = 0)$; (b) Phase angles of the transverse displacement spectra for the constrained composite damping plate with two piezoelectric layers driven by a point force at 1.5kHz, $\left(G_p = 200, G_d = 0.2\right)$, $(x_0 = 0, y_0 = 0)$

4 Conclusions

The governing equations of the constrained composite damping plates with double piezoelectric layers are derived in the wavenumber domain by using classical laminated plate theory. The solutions of the three-dimensional electric potential equations for smart layers with open circuit, closed circuit, external dielectric slab and active control are developed. Five governing equations for thin smart composite plates are obtained. The natural frequencies and loss factors of the constrained composite damping plate with two piezoelectric layers are analyzed. The vibrational features of smart composite plate using three different passive control methods are all very similar to free vibrations of the constrained composite damping plate without piezoelectric effects. Piezoelectric layers with passive control are not suitable to suppress vibrations of composite plate and to absorb mechanical energy. The natural frequencies and loss factors of the composite plates with active control behave markedly differently. The energy of the transverse displacement PPSD for the smart composite plates with active control is reduced. The CSD of the transverse displacement for the constrained composite damping plate with uniform layers is composed of cylindrical waves with circumferential wavenumber 0 and only the flexural waves with even circumferential wavenumber contribute to the CSD of the composite plate with orthotropic layer driven by the force located at the origin. The patterns of the CSD for the constrained composite damping plates are changed by the force location but those of RPSD for

the composite plates are independent of the force location. The phase angles of the transverse displacement spectra are greatly affected by the force position and damping.

Acknowledgment

The first author is grateful for the invitation and support from the School of Mathematical Sciences, University of Nottingham during his stay as a visiting scholar from Shanghai Maritime University. This study is supported by the National Natural Science Foundation of China (11302124) and the Doctoral Subject Foundation of China's Education Ministry (20133121120003).

References

[1] S.C. Kattimani, M.C. Ray, Vibration control of multiferroic fibrous composite plates using active constrained layer damping, Mechanical Systems and Signal Processing 106 (2018) 334-354.

[2] I.Y. Shen, Active constrained layer damping treatments for shell structures: a deep-shell theory, some intuitive results, and an energy analysis, Smart Materials and Structures 6 (1) (1997) 89-101.

[3] X.N. Zhang, J.H. Zhang, The hybrid control of vibration of thin plate with active constrained damping layer, Applied Mathematics and Mechanics (English Edition) 19 (12) (1998) 1119-1134.

[4] J.X. Gao, Y.P. Shen, Vibration and damping analysis of a composite plate with active and passive damping layer, Applied Mathematics and Mechanics (English Edition) 20 (10) (1999) 1075-1086.

[5] C.H. Park, A. Baz, Newtonian and variational formulations of the dynamics of plates with active constrained layer damping treatments, Journal of Vibration and Control 10 (3) (2004) 399-421.

[6] L.Y. Yuan, Y. Xiang, Y.Y. Huang, J. Lu, A semi-analytical method and the circumferential dominant modal control of circular cylindrical shells with active constrained layer damping treatment, Smart Materials and Structures 19 (2) (2010) 1-14.

[7] Y. Xiang, Y.Y. Huang, J. Lu, L.Y. Yuan, S.Z. Zou, New matrix method for analyzing

vibration and damping effect of sandwich circular cylindrical shell with viscoelastic core, Applied Mathematics and Mechanics (English Edition) 29 (12) (2008) 1587-1600.

[8] H.Y. Zhang, Y.P. Shen, Vibration suppression of laminated plates with 1-3 piezoelectric fiber-reinforced composite layers equipped with interdigitated electrodes, Composite Structures 79 (2) (2007) 220-228.

[9] A.E. Guennam, B.M. Luccioni, Model for piezoelectric/ferroelectric composites polarized with interdigitated electrodes, Composite Structures 131 (2015) 312-324.

[10] X. Yuan, Z.Q. Chen, M.L. Wu, H. Luo, C. Chen, K.C. Zhou, D. Zhang, A novel thickness polarized d_{15} shear piezoelectric fiber composites, Sensors and Actuators A: Physical 260 (2017) 185-190.

[11] V.A. Akop'yan, A.V. Nasedkin, E.V. Rozhkov, A.N. Solovjev, S.N. Shevtsov, Influence of the geometry and connection of electrodes on electromechanical characteristics of frequency-tuned disk piezoelectric elements, Russian Journal of Nondestructive Testing 42 (5) (2006) 334-339.

[12] S.B. Chen, G. Wang, J.H. Wen, X.S. Wen, Wave propagation and attenuation in plates with periodic arrays of shunted piezo-patches, Journal of Sound and Vibration 332 (6) (2013) 1520-1532.

[13] H. Zhang, J.H. Wen, Y. Xiao, G. Wang, X.S. Wen, Sound transmission loss of metamaterial thin plates with periodic subwavelength arrays of shunted piezoelectric patches, Journal of Sound and Vibration 343 (2015) 104-120.

[14] K.J. Yi, L. Li, M. Ichchou, M. Collet, Sound insulation performance of plates with interconnected distributed piezoelectric patches, Chinese Journal of Aeronautics 30 (1) (2017) 99-108.

[15] W. Larbi, L.P. da Silva, J.F. Deü , An efficient FE approach for attenuation of acoustic radiation of thin structures by using passive shunted piezoelectric systems, Applied Acoustics 128 (2017) 3-13.

[16] Z. Zhang, S. Li, Q. Huang, Low-frequency sound radiation of infinite orthogonally ribstiffened sandwich structure with periodic subwavelength arrays of shunted piezoelectric patches, Composite Structures 187 (2018) 144-156.

[17] M.C. Ray, J.N. Reddy, Optimal control of thin circular cylindrical laminated composite shells using active constrained layer damping treatment, Smart Materials and Structures 13 (1) (2004) 64-72.

[18] R. Suresh Kumar, M.C. Ray, Active control of geometrically nonlinear vibrations of doubly curved smart sandwich shells using 1-3 piezoelectric composites, Composite Structures 105 (2013) 173-187.

[19] J. Lu, P. Wang, Z. Zhan, Active vibration control of thin-plate structures with partial SCLD treatment, Mechanical Systems and Signal Processing 84 (2017) 531-550.

[20] J.S. Moita, A.L. Araújo, V.F. Correia, C.M. Mota Soares, J. Herskovits, Active-passive damping in functionally graded sandwich plate/shell structures, Composite Structures 202 (2018) 324-332.

[21] S.C. Kattimani, M.C. Ray, Smart damping of geometrically nonlinear vibrations of magneto-electro-elastic plates, Composite Structures 114 (2014) 51-63.

[22] A.L. Arasjo, V.S. Carvalho, C.M. Mota Soares, J. Belinha, A.J.M. Ferreira, Vibration analysis of laminated soft core sandwich plates with piezoelectric sensors and actuators, Composite Structures 151 (2016) 91-98.

[23] S. Carra, M. Amabili, R. Ohayon, P.M. Hutin, Active vibration control of a thin rectangular plate in air or in contact with water in presence of tonal primary disturbance, Aerospace Science and Technology 12 (1) (2008) 54-61.

[24] G. Ferrari, M. Amabili, Active vibration control of a sandwich plate by non-collocated positive position feedback, Journal of Sound and Vibration 342 (2015) 44-56.

[25] J. Yang, J. Xiong, L. Ma, B. Wang, G. Zhang, L. Wu, Vibration and damping characteristics of hybrid carbon fiber composite pyramidal truss sandwich panels with viscoelastic layers, Composite Structures 106 (2013) 570-580.

[26] X. Liu, Q. Wang, S.T. Quek, Analytical solution for free vibration of piezoelectric coupled moderately thick circular plates, International Journal of Solids and Structures 39 (8) (2002) 2129-2151.

[27] M.C. Ray, Optimal control of laminated shells using piezoelectric sensor and actuator layers, AIAA Journal 41 (6) (2003) 1151-1157.

[28] F. Ebrahimi, A. Rastgoo, A.A. Atai, A theoretical analysis of smart moderately thick shear deformable annular functionally graded plate, European Journal of Mechanics A/Solids, 28 (5) (2009) 962-973.

[29] G.G. Sheng, X. Wang, Active control of functionally graded laminated cylindrical shells, Composite Structures 90 (4) (2009) 448-457.

[30] S. Hosseini-Hashemi, M. Es'haghi, H. Rokni Damavandi Taher, An exact analytical solution for freely vibrating piezoelectric coupled circular/annular thick plates using Reddy plate theory, Composite Structures 92 (6) (2010) 1333-1351.

[31] Y.Q. Mao, Y.M. Fu, Nonlinear dynamic response and active vibration control for piezoelectric functionally graded plate, Journal of Sound and Vibration 329 (11) (2010) 2015-2028.

[32] A. Alibeigloo, A.M. Kani, M.H. Pashaei, Elasticity solution for the free vibration analysis of functionally graded cylindrical shell bonded to thin piezoelectric layers, International Journal of Pressure Vessels and Piping 89 (2012) 98-111.

[33] Z.G. Song, F. M. Li, Active aeroelastic flutter analysis and vibration control of supersonic composite laminated plate, Composite Structures 94 (2) (2012) 702-713.

[34] A. Alibeigloo, Three-dimensional thermoelasticity solution of functionally graded carbon nanotube reinforced composite plate embedded in piezoelectric sensor and actuator layers, Composite Structures 118 (2014) 482-495.

[35] N.D. Duc, T.Q. Quan, V.D. Luat, Nonlinear dynamic analysis and vibration of shear deformable piezoelectric FGM double curved shallow shells under damping-thermo-electro-mechanical loads, Composite Structures 125 (2015) 29-40.

[36] S.M. Hasheminejad, V. Rabbani, Active transient sound radiation control from a smart piezocomposite hollow cylinder, Archives of Acoustics 40 (3) (2015) 359-381.

[37] A. Fereidoon, E. Andalib, A. Mirafzal, Nonlinear vibration of viscoelastic embedded-DWCNTs integrated with piezoelectric layers-conveying viscous fluid considering surface effects, Physica E: Low-dimensional Systems and Nanostructures 81 (2016) 205-218.

[38] B.A. Selim, L.W. Zhang, K.M. Liew, Active vibration control of FGM plates with piezoelectric layers based on Reddy's higher-order shear deformation theory, Composite Structures 155 (2016) 118-134.

[39] A. Alibeigloo, A.A. Pasha Zanoosi, Thermo-electro-elasticity solution of functionally graded carbon nanotube reinforced composite cylindrical shell embedded in piezoelectric layers, Composite Structures 173 (2017) 268-280.

[40] H. J. Jiang, L. H. Liang, L. Ma, J. Guo, H. L. Dai, X. G. Wang, An analytical solution of three-dimensional steady thermodynamic analysis for a piezoelectric laminated plate using refined plate theory, Composite Structures 162 (2017) 194-209.

[41] R. Kolahchi, M.S. Zarei, M.H. Hajmohammad, A. Nouri, Wave propagation of embedded viscoelastic FG-CNT-reinforced sandwich plates integrated with sensor and actuator based on refined zigzag theory, International Journal of Mechanical Sciences 130 (2017) 534-545.

[42] B.A. Selim, L.W. Zhang, K.M. Liew, Active vibration control of CNT-reinforced composite plates with piezoelectric layers based on Reddy's higher-order shear deformation theory, Composite Structures 163 (2017) 350-364.

[43] E. Arshid, A.R. Khorshidvand, Free vibration analysis of saturated porous FG circular plates integrated with piezoelectric actuators via differential quadrature method, Thin-Walled Structures 125 (2018) 220-233.

[44] A. Zippo, G. Ferrari, M. Amabili, M. Barbieri, F. Pellicano, Active vibration control of a composite sandwich plate, Composite Structures 128 (2015) 100-114.

[45] H. Yue, Y. Lu, Z. Deng, H. Tzou, Experiments on vibration control of a piezoelectric laminated paraboloidal shell, Mechanical Systems and Signal Processing 82 (2017) 279-295.

[46] P. Cupiał, J. Niziol, Vibration and damping analysis of a three-layered composite plate with a viscoelastic mid-layer, Journal of Sound and Vibration 183 (1) (1995) 99-114.

[47] M. Meunier, R.A. Shenoi, Dynamic analysis of composite sandwich plates with damping modelled using high-order shear deformation theory, Composite Structures 54 (2) (2001) 243-254.

[48] M. Meunier, R.A. Shenoi, Forced response of FRP sandwich panels with viscoelastic materials, Journal of Sound and Vibration 263 (1) (2003) 131-151.

[49] C. Yang, G. Jin, Z. Liu, X. Wang, X. Miao, Vibration and damping analysis of thick sandwich cylindrical shells with a viscoelastic core under arbitrary boundary conditions, International Journal of Mechanical Sciences 92 (2015) 162-177.

[50] S.C. Huang, C.Y. Tsai, C.L. Liou, A general vibration theory for constrained layer damping-treated thick sandwich structures, Journal of Sandwich Structures and Materials 18 (3) (2016) 343-373.

[51] X.Q. Zhou, D.Y. Yu, X.Y. Shao, S.Q. Zhang, S. Wang, Asymptotic analysis on flexural dynamic characteristics for a laminated composite plate with embedded and perforated periodically viscoelastic damping material core, Composite Structures 154 (2016) 616-633.

[52] X.Q. Zhou, D.Y. Yu, X.Y. Shao, S. Wang, S.Q. Zhang, Asymptotic analysis for composite laminated plate with periodically fillers in viscoelastic damping material core, Composites Part B: Engineering 96 (2016) 45-62.

[53] M. Arafa, A. Baz, Energy-dissipation characteristics of active piezoelectric damping composites, Composites Science and Technology 60 (15) (2000) 2759-2768.

[54] S.C. Yu, S.C. Huang, Vibration of a three-layered viscoelastic sandwich circular plate, International Journal of Mechanical Sciences 43 (10) (2001) 2215-2236.

[55] H.J. Wang, L.W. Chen, Vibration and damping analysis of a three-layered composite annular plate with a viscoelastic mid-layer, Composite Structures 58 (4) (2002) 563-570.

[56] L.F. Li, X.Z. Wang, Y.H. Zhou, Dynamic characteristics of traveling waves for a rotating laminated circular plate with viscoelastic core layer, Journal of Sound and Vibration 330 (12) (2011) 2836-2847.

[57] H.J. Wang, L.W. Chen, Axisymmetric dynamic stability of rotating sandwich circular plates, Journal of Vibration and Acoustics 126 (3) (2004) 407-415.

[58] X.Z. Wang, L.F. Li, Y.H. Zhou, Aeroelastic dynamics stability of rotating sandwich annular plate with viscoelastic core layer, Applied Mathematics and Mechanics (English Edition) 37 (1) (2016) 107-120.

[59] X.T. Cao, L. Shi, X.S. Zhang, G.H. Jiang, Active control of acoustic radiation from laminated cylindrical shells integrated with a piezoelectric layer, Smart Materials and Structures 22 (6) (2013) 065003.

[60] C.H. Park, A. Baz, Comparison between finite element formulations of active constrained layer damping using classical and layer-wise laminate theory, Finite Elements in Analysis and Design 37 (1) (2001) 35-56.

[61] X.T. Cao, H.X. Hua, Sound radiation from shear deformable stiffened laminated plates with multiple compliant layers, Journal of Vibration and Acoustics 134 (5) (2012) 051001.

[62] D. Chronopoulos, M. Ichchou, B. Troclet, O. Bareille, Computing the broadband vibroacoustic response of arbitrarily thick layered panels by a wave finite element approach, Applied Acoustics 77 (2014) 89-98.

[63] M.Amabili, S.Farhadi, Shear deformable versus classical theories for nonlinear vibrations of rectangular isotropic and laminated composite plates, Journal of Sound and Vibration 320 (3) (2009) 649-667.

[64] M. Amabili, Nonlinear vibrations of laminated circular cylindrical shells: comparison of different shell theories, Composite Structures 94 (1) (2011) 207-220.

[65] M. Amabili, J.N. Reddy, A new non-linear higher-order shear deformation theory for large-amplitude vibrations of laminated doubly curved shells, International Journal of Non-Linear Mechanics 45 (4) (2010) 409-418.

[66] A.A. Khdeir, Comparison between shear deformable and Kirchhoff theories for bending, buckling and vibration of antisymmetric angle-ply laminated plates, Composite Structures 13 (3) (1989) 159-172.

[67] A.A. Khdeir, J.N. Reddy, Free vibrations of laminated composite plates using second-order shear deformation theory, Computers & Structures 71 (6) (1999) 617-626.

[68] J.N. Reddy, A.A. Khdeir, Dynamic response of cross-ply laminated shallow shells according to a refined shear deformation theory, Journal of the Acoustical Society of America 85 (6) (1989) 2423-2431.

[69] M.F. Liu, An exact deformation analysis for the magneto-electro-elastic fiber-reinforced thin plate, Applied Mathematical Modelling 35 (5) (2011) 2443-2461.

[70] X.T. Cao, Z.Y. Zhang, H.X. Hua, Free vibration of circular cylindrical shell with constrained layer damping, Applied Mathematics and Mechanics (English Edition) 32 (4) (2011) 495-506.

[71] L.H. Chen, S.C. Huang, Vibrations of a cylindrical shell with partially constrained layer damping (CLD) treatment, International Journal of Mechanical Sciences 41 (12) (1999) 1485-1498.

[72] H. Li, Y. Yang, Dynamic response and active control of a composite cylindrical shell with piezoelectric shear actuators, Smart Materials and Structures 16 (3) (2007) 909-918.

[73] M.C. Ray, J.N. Reddy, Active control of laminated cylindrical shells using piezoelectric fiber reinforced composites, Composites Science and Technology 65 (7-8) (2005) 1226-1236.

[74] K.Y. Lam, T.Y. Ng, Active control of composite plates with integrated piezoelectric sensors and actuators under various dynamic loading conditions, Smart Materials and Structures 8 (2) (1999) 223-237.

[75] W. Laplante, T.H. Chen, A. Baz, W. Shields, Active control of vibration and noise radiation from fluid-loaded cylinder using active constrained layer damping, Journal of Vibration and Control 8 (6) (2002) 877-902.

[76] E.A. Magliula, J.G. McDaniel, A.D. Pierce, Far-field approximation for a point-excited anisotropic plate, The Journal of the Acoustical Society of America 131 (6) (2012) 4535-4542.